The Draconic gearing of the Antikythera Mechanism

Assembling the Fragment D on the Antikythera Mechanism: Its role and operation

A.Voulgaris[1], C.Mouratidis[2], A.Vossinakis[3], G.Bokovos[4]

(Submitted 14 January 2020)

[1]Municipality of Thessaloniki, Directorate Culture and Tourism, Thessaloniki, GR-54625, Greece

[2]Hellenic Ministry of Education, Research and Religious Affairs, Kos, GR-85300, Greece

[3]Thessaloniki Astronomy Club, Thessaloniki, GR-54646, Greece

[4]Thessaloniki Science Center and Technology Museum-Planetarium, Thermi, GR-57001, Greece

Abstract

The unplaced Fragment D of the Antikythera Mechanism with unknown operation, was a mystery since the beginning of its discovery. The gear r1, which was detected on the Fragment radiographies by C. Karakalos, is preserved in very good condition, but this was not enough to correlate it to the existing gear trainings of the Mechanism. According to recent researches and observations, the planet gearing indication on the Antikythera Mechanism is not probable, so the operation and position of gear r1, was still unknown. Based on Fragment A gearing trains, an ideal operation and proper position of this enigmatic gear/part of the Mechanism, is presented, analyzed and discussed, taking into account all of the mechanical characteristics and the other two parts of the Fragment D, visible in AMRP tomographies. The described operation and position of Fragment D, gives answers on several questions and improves the Mechanism functionality, contributing to the completion of the Antikythera Mechanism puzzle.

1. Introduction. The Antikythera Mechanism, a geared machine based on the lunar cycles

The Antikythera Mechanism, a creation of an ingenious manufacturer of the Hellenistic era, was a geared machine capable of performing complex astronomical calculations, based on the periodic cycles of the moon and the sun. After 2000 years under the Aegean/Ionian sea (Jones 2017; Voulgaris et al., 2019b), the Antikythera Mechanism is now a permanent exhibit at the National Archaeological Museum of Athens, Greece.

At the Ancient Greece era, time calculations and predictions were directly correlated to the astronomical events and the position in the sky of the two celestial bodies, the Moon and the Sun. The astronomical events regulated the everyday life and human activities such as agricultural works, religious holidays, sacrifices to the gods, navigation etc. (Lehoux 2012; Anastasiou et al., 2013)

At the ancient time, the lunar cycles were used as the main calendar *time units* (Hannah 2013). Each month of the ancient Greek calendar begun with the New Moon, so the basic time unit was the synodic month (Bowen and Goldstein 1988; Hannah 2013). Even the Olympic Games started on the 8^{th} or 9^{th} Full Moon after the Winter Solstice (Vaughan 2002). Although one tropical year does not include an integer number of lunar synodic months, the lunar cycle prevailed instead of the tropical year, which was considered less important.

It was Meton, a Greek mathematician and astronomer, based on older observations from the Babylonian astronomers (Bowen and Goldstein 1988; Danezis and Theodosiou 1995), that introduced a calendar using an integer number of 235 lunar synodic cycles (also 254 sidereal cycles), which is equal to the integer number of 19 tropical years, known as "*enneakedekaeteris*". Each Metonic year of 12 or 13 synodic months deviated from the actual start of the tropical year by several days, in order to keep the lunar synodic month intact (Geminus 1880 and 2002; Anastasiou et al., 2016a).

The lunar cycles were chosen by the ancient astronomers and the "*time keepers*", instead of the solar cycles for a number of obvious reasons: it's easy to calculate a time span based on the moon's every day changing phase, it is visible both at night and at day and it's easy to observe bright stars when the moon is up on the sky. In contrast, the Sun does not exhibit any phases, it is impossible to detect stars when the Sun is above the horizon and the relative position of the Sun on the sky changes by about $1/12^{th}$ of the lunar angular velocity. Also a special "solar phase", i.e. a solar eclipse, is a rare astronomical event to observe from a specific place. All of these slow *solar changes*, lead the ancient astronomers to base their measurements and time keeping events on the lunar cycle.

By studying the Antikythera Mechanism it is obvious that the operation, design and the gear teeth selection, were mostly based on the synodic lunar month: the b_{in} axis-Lunar Disc-Input (the fastest of the rotating axes), the small Lunar phases sphere on the Lunar Disc and the cells on the two spirals (Saros and Metonic), were all precisely based on the synodic lunar month. The selection of the teeth number of most of the gear trainings was chosen in accordance to the synodic and sidereal lunar cycles, e.g. the number of the gear teeth *e3* (223 synodic months of Saros) and (*c2/d1)*d2* (2 X 127 = 254 sidereal months of Metonic

cycle). The rotation of the Lunar Disc, which is the proper input for the Antikythera Mechanism gearing trains, essentially defines the two lunar cycles - the sidereal and synodic month - as the basic time units for the calculations of the Mechanism. Only two out of the seven pointers of the Mechanism are related to the tropical year: the Golden Sphere-Sun pointer (which was probably adapted directly to the perimeter of the annular gear *b1*, Voulgaris et al., 2018b) i.e. one full rotation equals to one tropical year, and the athletic games pointer (one rotation per 4 tropical years).
All of the above leads to the conclusion that the Antikythera Mechanism was a Luni-(solar) time/calendar geared machine computer, based on the lunar synodic cycle.

2. The Lunar motions studied in the Hellenistic era

The ancient Greek astronomers/geometers who had studied older observations by the Babylonians, Chaldeans and the Egyptians, continued the time measuring by observing and recording the positions of the celestial bodies (Evans 1998; Steele 2000; Hannah 2001; Steele 2002). We can assume that the ancient astronomers used an oblong, long length, papyrus with a central line calibrated with time subdivisions, representing the Ecliptic and with the zodiac constellation stars sketched, in which the astronomers noted the position of the Sun and the Moon every day. Obviously the study of this papyrus revealed the “strange” movement (anomaly) of the Moon relative to the stars and the Ecliptic. Based on these lunar movements, the astronomers introduced geometrical schemes/models using the line, the circle, the ellipse and the trigonometry, in order to represent the motions of the Moon (Ptolemy 1984).

The four well known lunar motions, the synodic, sidereal, anomalistic and draconic cycles, where extensively observed and studied by the ancient astronomers, in order to find out a correlation i.e. a periodic coincidence of the start of these periodic cycles. Ptolemy 1984, in Almagest extensively referred on the main lunar cycles, giving a large number of calculations in tables (Pedersen 2011). The attempt of Ptolemy, Hipparchus and the previous era astronomers to (better) correlate - incorporate the four lunar cycles, it was obvious.
The ancient astronomers realized that a correlation - phase synchronization (periodicity) of two of the four lunar motions/cycles, revealed a repeatability of the solar/lunar eclipses and the synchronization of three lunar cycles, presented eclipses with highly similar geometrical characteristics and classification (Oppolzer 1889; van den Bergh 1955; Meeus et al., 1966; Neugebauer 1975; Meeus 2004). The periodicity of the lunar motions, led to the adoption of

the "*interrelated cycles ratio in integer numbers*", a very useful canon, which was the key for the solar/lunar eclipses prediction. Ptolemy refers to the Saros cycle with the name "Periodic*", … since it is the smallest single period which contains an integer number of returns of the various motions*" (Ptolemy 1984).

Of course the most easily observed lunar cycle was the synodic month, i.e. the time span between two successive New Moons or Full Moons, which was easily measured with sufficient accuracy Fig. 1A,D. For this reason, the rest three of the lunar cycles were calculated based on the synodic month.

The sidereal month is the time duration when the Moon returns approximately to the same star Fig. 1A,C, but the start of each cycle presents a different lunar phase. Moreover, it's difficult to identify the start of each cycle: the daylight or the Full Moon light can erase the light of the nearby stars, making difficult the observations and the measurements.

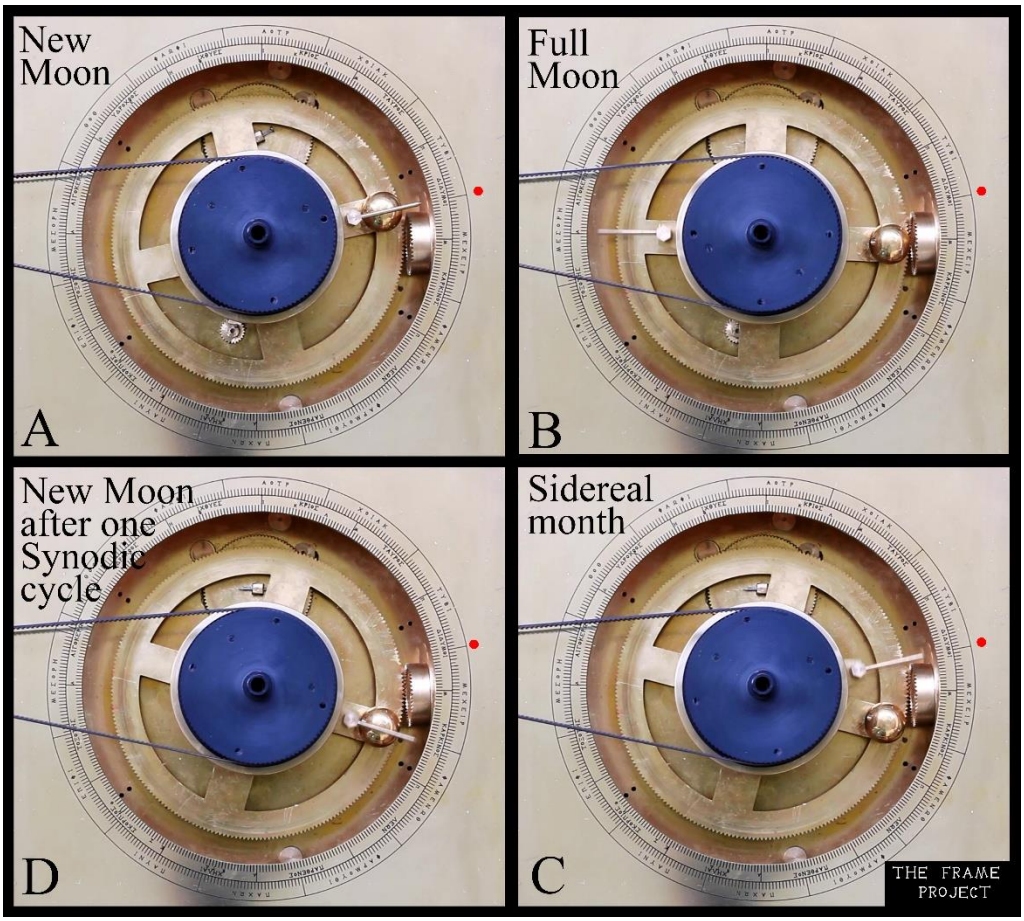

Figure 1: A pulley is adapted on the Lunar Disc of the Antikythera Mechanism functional model (designed/constructed by the FRAMe Project) and an electrical motor rotates the Lunar Disc via a belt (images taken from video frames). The position/phases of the Moon relative to the Golden sphere-Sun and the zodiac sky, are presented. A) The red dot that marks the Egyptian month of 1st MECHIR (ΜΕΧΕΙΡ), also the 18th zodiac day of Gemini (ΔΙΔΥΜΟΙ) is the starting position of the Lunar Disc and the Golden sphere. B, C, D) During the rotation of the Lunar Disc, the Golden sphere continuously

changes its position relative to the zodiac sky (the small mismatch of the aiming, is a cause of the parallax error during the video recording). Each synodic month on the Antikythera Mechanism, started with the Full Moon phase (see Chap. 4).

The anomalistic month, became evident by the variable, (increased-decreased) angular velocity of the moon in relation to the fixed stars. Geminus 2002 (Evans and Berggren 2006), refers that the minimum angular velocity is 11° 06' 35" per day, at the start of the anomalistic month (apogee) and the maximum is 15° 14' 35" per day, measured on the middle of the anomalistic month (perigee). Of course this angular variation is not easily detected without the use of an astronomical instrument (astrolabe) and by recording a number of observations and measurements, as Ptolemy presents in Almagest. Geminus also describes the mathematical process for the calculation of the mean lunar angular velocity and also refers the measuring error, as a result of the specific resolution of the instrument used.

The variable lunar motion is also included on the Antikythera Mechanism (Freeth et al., 2006), which is introduced by the operation of the *pin&slot* design on the gears *k1*/*k2* (Wright 2006; Gourtsoyannis 2010; Voulgaris et al., 2018b). The centers of gears *k1* and *k2* are located in "*off axis*" position and the movement transmission, from gear *k2* (slot) to *k1* (pin), presents a variable angular velocity, with values equal to the lunar variable motion.

The fourth, more complex lunar motion is the continuous change of the position of the two lunar Nodes: The elliptical lunar orbit plane has an inclination to the Ecliptic about 5.15° and crosses the Ecliptic plane on two points, named Ascending and Descending Node. The line connecting the two Nodes, named Line of Nodes Fig. 2. The ancient astronomers, in order to justify the "strange" ecliptic latitude changes of the projected lunar movements in the sky, (correctly) introduced the model of the slow retrograde rotation of the Line of Nodes.

Ptolemy 1984 in Almagest calls the time span in which the Moon crosses the same Node, as "*Ἀποκατάστασις ἀνωμαλίας κατά πλάτος" (return to the same latitude)*, better known as *draconic* or *draconitic month* (by the Middle Ages myth of the Dragon which "eats" the sun during a solar eclipse, see Kircher 1646, page 548), also known as *nodal* or *nodical month*. The duration of the draconic month is about 27.2122^{d}, a bit shorter than the sidereal month (27.3218^{d}) Barbieri 2017. The two Nodes return to the same position relative to the stars, after 18.612 tropical years (a bit larger than a Saros cycle, see Espenak and Meeus, 2008-NASA eclipse page). This means that the Nodes change their projected position on the sky, by about 1.564°/1 synodic month. Therefore, the Line of Nodes transits each constellation in about 19.2 synodic months.

The draconic month is directly correlated to the solar/lunar eclipses: if at the start (first Node) or the middle (second Node) of the draconic month, there is a New Moon or a Full Moon, then a solar or a lunar eclipse will occur.

One hundred years after Meton, Callippus based on his observations, improved the Metonic cycle into a more precise correlation between the lunar synodic cycles to the solar tropical year, known as a Callippic cycle (Waerden 1984b), which started on the New Moon and the Summer Solstice of 28 June 330 BC. On about 100 BC, Hipparchus further corrected the Callippic cycle, calculating a better approximation to the integer number ratio of the synodic month and the tropical year.

Table I: *The time measuring cycles measured in days and the corresponding duration in tropical years, as recorded by the observations of Babylonians and the ancient Greek astronomers. True and rounded values of the draconic month are presented. Note that 1/1000 of a synodic month is about 42.5 minutes. The ratio of draconic to synodic month is rounded to 1.08520.*

Cycle (invented for…)	**Tropical years**	**Number of Days**	**Days per Year**	**Synodic months**	**Draconic months** (rounded)	**Ratio Draconic/ Synodic month**	**Draconic month** (days)
Saros (eclipses)	$18^{y}\ 11.3^{d}$	6585.322	365.2233	223	242	1.0852017	27.212074
					241.999 (true)	1.0851973	27.212186
Metonic (tropical year)	19^{y}	6940	365.2631	235	255	1.0851063	27.215686
					255.021 (true)	1.0851957	27.213445
Exeligmos (eclipses)	$54^{y}\ 33^{d}$	19756	365.2235	669	726	1.0852017	27.212121
					725.996 (true)	1.0851958	27.212271
Callippic (tropical year)	76^{y}	27759	365.25	940	1020	1.0851063	27.214705
					1020.84 (true)	1.0851957	27.192312
Hipparchic (tropical year)	345^{y}	126010	365.246	4267	4630.5	1.0851886	27.213043
					4630.531 (true)	1.0851959	27.212861
Babylonian (eclipses)	$441^{y}\ 106.3^{d}$	161188	365.2646	5458	5923	1.0851960	27.213911
					5922.999 (true)	1.0851958	27.213916

From **Table I** it can be seen that there is no satisfying relation of an integer number of draconic months to the tropical year cycles. The Metonic, Callippic and Hipparchic cycles

were invented in order to better correlate the synodic month to the tropical year (Oppolzer 1889; Meeus et al., 1966; Neugebauer 1975; Meeus 2004). Saros and Exeligmos, which remained unchanged to further corrections in future time (after Hipparchus), offer a better correlation to integer numbers between the draconic and the synodic cycle, but not for the tropical year and for this reason were the proper cycles for the eclipse predictions.

3. Necessary Parameters for a solar/lunar eclipse - The Draconic cycle

One of the most important astronomical events in antiquity and also today, is a solar eclipse (https://www.greatamericaneclipse.com/basics, https://sites.williams.edu/eclipse/2019-chile/). In ancient Mesopotamia, Egypt and Greece, eclipses were correlated to an extended mythology, regarding the fight of Gods, the Kings and their thrones, dragons eating the sun, superstitions etc. In China of 2300 BC, the astronomers Hi and Ho were executed, because they failed to predict a solar eclipse (Brown 1931). The war between Medes and Lydians stopped during the eclipse of 28 May 585 BC, which was predicted by Thales (Panchenko 1994; Stephenson and Fatoohi 1997; Herodotus 1998). Therefore, the prediction of a solar eclipse was a great challenge for the astronomers of the ancient world, who used their observations and calculations, in order to improve the accuracy of the eclipse predictions (Steele 2015).

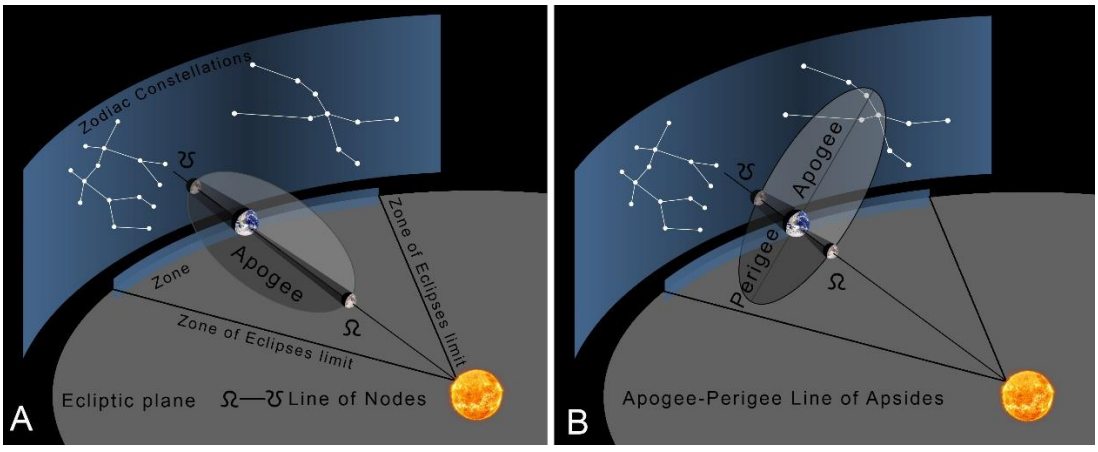

Figure 2: The cross section of the elliptical lunar orbit plane to the Ecliptic plane (not in scale). The limits of the Zone of Eclipses, are also presented. A) The Moon in apogee crosses the Ascending Node (i.e. the Draconic and the Anomalistic month start simultaneously). B) 60.5 draconic months (55.75 synodic months) before, the Moon crosses the two Nodes with its mean velocity. Note that during a solar eclipse the corresponding Node is projected to (or close to) the same zodiac degree (constellation point) in which the Sun is located and during a lunar eclipse, the corresponding Node is projected to the opposite constellation point than the Sun. Schemes by the authors.

A solar/lunar eclipse will occur, only if two specific astronomical positional parameters are satisfied:

1) The Moon is at its new phase (*corresp.* Full Moon), i.e. on the start (half) of the synodic month and

2) At the same time, the New Moon (*corresp.* Full Moon) is located at (or close) to the Ascending or the Descending Node, i.e. close to the beginning (*corresp.* middle) of the draconic month Fig. 2.

The resonance of these two periods in about 0 or 2π phase, guarantees that somewhere on the Earth, a solar (lunar) eclipse will happen Fig. 3. Of course, in order to predict where on Earth the eclipse will be visible, additional calculations and parameters is needed.

If the three celestial bodies were point-like, an eclipse would occur only when the New (Full) moon exactly crosses one of the Nodes. Because the moon and the Earth have angular dimensions of about 0.5° for the moon as observed from the Earth and about 1.5° for the Earth as observed from the Moon, their corresponding shadows are extended. So, an eclipse can occur even if the moon is located in an angular distance from the Node. This way a zone on the Ecliptic can be defined with angular dimensions of about ±17° 25’ on either side of the Nodes, called the *Zone of Eclipses*. The ecliptic limits vary depending on the angular dimensions of the Moon, as a result of its varying distance from the Earth (perigee and apogee) i.e. by the Anomalistic cycle Fig. 4. The exact phase of the anomalistic cycle (perigee/apogee position) during the resonance of the synodic and draconic cycles, defines the type of the eclipse event (total, annular or hybrid, also less affected by the Earth’s apogee/perigee), (Espenak and Meeus, 2008-NASA eclipse page) and the exact time in which the moon approaches the Nodes or crosses the ecliptic limits, acting as a variable timer (see chap. 7.3).

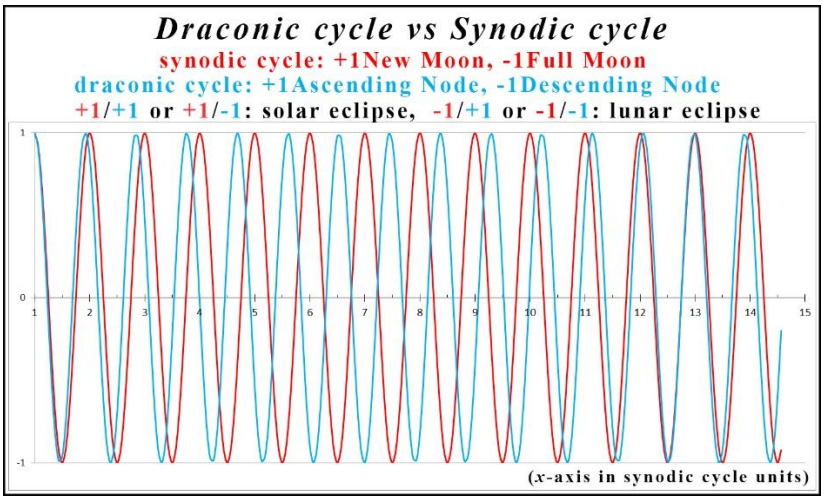

Figure 3: Harmonic graph of the draconic vs synodic cycle, assuming that the two cycles start simultaneously. On each of the resonance (or close to resonance) points (phase π or 2π) of the two graphs, a solar or lunar eclipse will occur. The units on the x-axis are synodic lunar cycles. (On the calculations for the graph presentation, the phase variation as a result of the anomalistic cycle, was not included).

The lower half area of the Back plate of the Antikythera Mechanism was dedicated on the eclipse events information (Freeth et al., 2008; Anastasiou et al., 2016b; Freeth 2019; Iversen and Jones 2019), presented on the Saros four turns spiral, divided in 223 cells (synodic months). The ancient manufacturer calculated, designed and constructed the proper gear training for this operation and at the same time he knew the information regarding the sequence of eclipses and the time they occur, which was engraved on the corresponding cells.

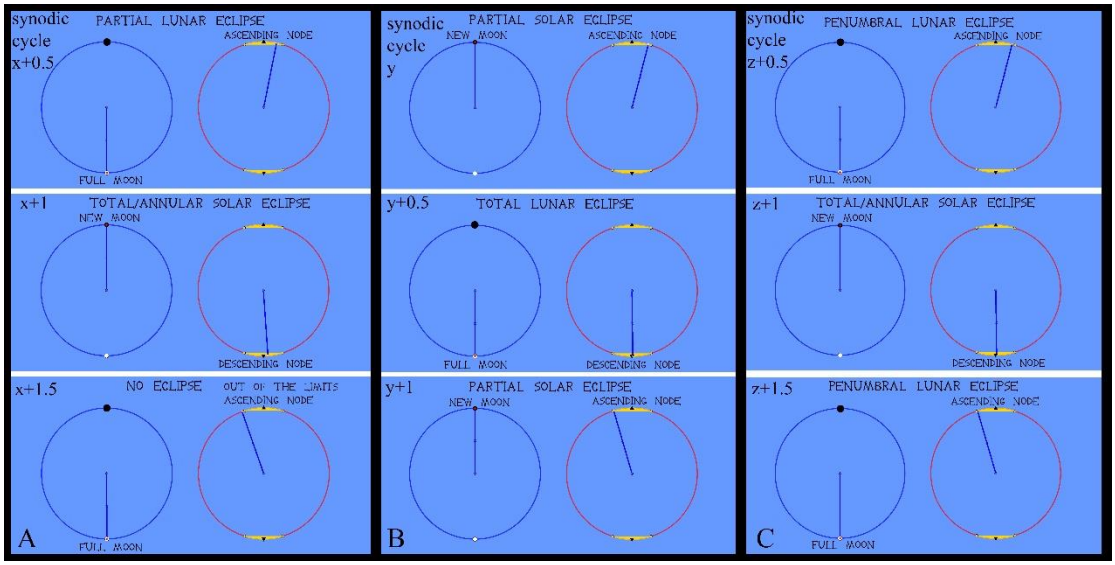

Figure 4: *Graphic representation of characteristic eclipse event sequences, occurring in a time span of 1.5 synodic month, based on the synodic and the draconic cycle. For the two cycles representation, Geogebra software was used. The Zone of Eclipses is presented in yellow color. Column A, The total solar eclipse of 11th August 1999, on which the Sun and the Moon were located close to the Ascending Node (retracted data from the Starry Night planetarium software). One fortnight (half synodic month) before this eclipse, on 28th July 1999, a partial lunar eclipse. One fortnight after the solar eclipse, on 27th August 1999 no lunar eclipse occurred, because the Moon was out of the Zone of Eclipses limit. Column B, The total lunar eclipse of 26th June 2029 will be accompanied with the two symmetrical partial solar eclipses (12th June and 11th July), visible from the north and south poles of the Earth.*
Column C, The annular solar eclipse of 21th June 2020 will occur when the Sun and the Moon are located just on the Ascending Node. This eclipse will be accompanied by two symmetrical penumbral lunar eclipses: A fortnight before, on 5th June 2020 and one fortnight after the solar eclipse, on 5th July 2020.

4. Eclipses information/prediction mechanism on the Antikythera Mechanism

The Antikythera Mechanism could predict with relative high accuracy, the main phases of the Moon and the position of the Sun on the sky (zodiac constellation) at the corresponding zodiac and metonic months (Voulgaris et al., 2018a). The user of the Mechanism, by turning the Lunar Disc, the proper in handling, input of the Mechanism (Voulgaris et al., 2018b), he could observe when the lunar pointer aimed directly to the Golden sphere (or on the opposite position). At these positions the small half white/half blackened lunar phase sphere of the Lunar Disc, shows its black (white) hemisphere (Wright 2006; Carman and Di Cocco 2016; Voulgaris et al., 2018b).

Although the ancient Greek months started at the day of New Moon and the day of Full Moon occurred in mid-month, Διχόμηνις (Theodosiou and Danezis 1995), this is not the case on the Antikythera Mechanism:

On the Saros spiral a number of pairs of successive cells are preserved, presenting eclipse events on synodic months Fig. 5 (cells 25-26, 78-79 and 119-120, Anastasiou et al., 2016, Freeth 2018). Let's assume that each cell (synodic month) of the Saros spiral begins at New Moon. When the Saros pointer aims to the *cell-25*, a solar eclipse on the 1st day of the month will occur. On the next *cell-26*, a lunar eclipse will occur at mid-month of the next month. The time span between the two events is 29.53^{d}+14.765^{d} = 44.295^{d} = 1.627 draconic month. A period of 1.5 draconic month, includes four successive Node transits (or four Nodes +/-x°, with x≤17°), in time duration of 40.818^{d}. So, the solar eclipse of the *cell-25* will occur when the Moon is on the first Node (or on Node +/-x°). Therefore, after 1.5 draconic month, i.e. when the moon crosses the second Node (fourth successive crossing), the moon phase is 44.295^{d} - 40.818^{d} = 3.477^{d} before the Full Moon phase referred on the *cell-26*, i.e. 14.765^{d} - 3.477^{d} = a waxing moon of 11.288^{d} crosses the second Node and therefore a lunar eclipse event is impossible to occur.

So, if each synodic month/cell starts at the time of New Moon, then the sequence "*solar eclipse in cell x and lunar eclipse in cell x+1, (i.e. next synodic month)*, is impossible to occur. One could argue that to resolve this problem, the rotation of the Saros pointer should be CCW, but the rotation of this pointer is definitely CW, as resulted by the index numbering of the Saros events, which increases in CW direction (Freeth et al., 2008; Anastasiou et al., 2016b).

This problem is totally resolved, if each of the 223 Saros cells-synodic months, starts at the time of Full Moon. Therefore, when the Saros pointer aims to the *cell-1* (begin of the Saros spiral), the Lunar Disc pointer must be in opposite direction to the Golden sphere (Full Moon). This result also explains why on the preserved cells with two eclipse events (Σ/H,

cells 125, 131, 137, 172, 178, and 184, Freeth et al., 2008; Anastasiou et al., 2016b), the ancient manufacturer engraved the lunar eclipse event (Σ) on the top and the solar eclipse event (H) on the bottom Fig. 5.

The start of each synodic month at the New Moon phase, presents a difficulty on the precise calculation of the 1st day of the month: because the New Moon is not visible and also the 2^{d} or 28^{d} phase moon are too close to the sun - practically non visible - there is an indeterminacy of about ±2.5 days of the exact day that the new month begins. Because of this five day gap, the date of the start of the month, can only be calculated indirectly. On the other side, the lunar phase of ±1^{d} from the full moon, can be easily resolved by naked eye observation. It seems that the ancient manufacturer took into account the practical-visual observations for the designing of his creation.

By each re-aiming of the Lunar Disc pointer to the Golden sphere (*corresp.* in opposite position-Full Moon), there was a possibility that a solar (*corresp.* lunar) eclipse would occur. By only observing the Front dial plate of the Mechanism, it was not possible to know for sure if a solar or a lunar eclipse would occur. Information about upcoming eclipses was only presented on the Saros spiral, on the Back plate of the Mechanism (Freeth et al., 2008; Anastasiou et al., 2016b). Therefore, after the re-aiming of the Lunar pointer to the Golden sphere, the user should check the Saros spiral, to see if the Saros pointer was located inside one of the 223 cells, in which there were the corresponding eclipse event inscriptions. So, the eclipse events of the Mechanism are detected only by observing the Saros pointer. It seems that the calculation of the draconic cycle, which is necessary for the eclipses prediction, is missing from the Antikythera Mechanism.

Let's study the "*nature*" of the Antikythera Mechanism, as a measuring instrument. The synodic month was presented on the Antikythera Mechanism by several indications. According to **Table II** it is obvious that the ancient manufacturer constructed this machine-time calculator, by utilizing two different speeds on its outputs. The Front plate pointers are *High Speed*/*High resolution* pointers, whereas the Back plate pointers are *Low speed*/*Low resolution*.

For example, the *High Speed* pointer of the Lunar Disc rotates about 389° in order to complete one synodic month (360° for one sidereal month) Fig. 1. This means that the pointer moves relatively fast, making a large travel in one lunar month, thus offering a *High Resolution* information of its position (of all the Mechanism gears, the Lunar Disc rotated with the fastest angular velocity). The aiming of the Lunar Disc pointer to the Golden sphere can be achieved with very high accuracy by hand rotating the Lunar Disc (input). The *High*

Speed pointers of the Mechanism present results that are based on precise geometrical characteristics e.g. the Full moon phase is depicted when the Lunar Disc pointer and the Golden sphere pointer are in opposite direction (180°).

On the other hand, a large number of compressed information, is engraved on the scales of the *Low Speed* pointers: 235 words (months) on each cell of the Metonic spiral and a number of eclipse events on some of the 223 Saros spiral cells. Each Metonic cell (synodic month) of 29.53 days, has a mean dimension of about 7mm X 4mm and the pointer moves through this cell during 29.53 days. So, the Metonic pointer changes its position about 7.6°/29.53 days ≈0.257°/day, (6.4°/29.53 days for the Saros spiral) Fig. 5. It is of course totally impossible to detect/measure time in precision of days directly on each of the Metonic/Saros cells (7mm/29.53 ≈0.237mm/day).

By the above theoretical calculation it results that the minimum unit of time of the Metonic and the Saros spirals is one cell i.e. one synodic month, which is the minimum measurable unit. Therefore, it is impossible to measure time with an accuracy below this limit, e.g. if the pointer aims on the middle of the cell, this does not mean that the date is precisely middle month. This calculation "inconsistency" arises from the small dimension of each minimum unit, the engagement of the gears with triangular teeth shape, the gear periodic errors, the small precession of the training axes, the (small) off-center positioning of the central gear holes, the random teeth shape mismatches, the mechanical limits of the specific gear training etc. (Edmunds 2011; Jones 2017).

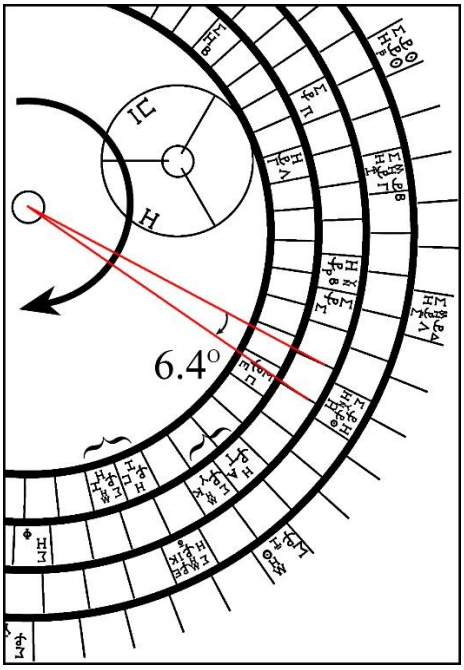

Figure 5: A close up of the Saros spiral with the eclipse information. The angle which the Saros pointer travels in one cell/synodic month is about 6.4°. Note also the two pairs of successive cells in which the

solar eclipse (H) is referred on the first cell and the lunar eclipse (Σ), on the next cell. Also, the cells with two eclipse events on the same synodic month, are visible (the lunar eclipse on the first line and the solar on the second line).

Such mechanical limits on the resolution, are present in all of the machines, even the optical instruments, such as telescopes, microscopes, spectrographs (resolution limits because of the diffraction of light, Hecht 2017). A simple paradigm for the above description is the resolution of the micrometer dial on the tool post slide hand-wheel (which moves the lathe support in *y*-axis): these subdivisions usually have a resolution of 0.025mm/subdivision line (or better) Fig. 6. This does not mean that in the middle between two lines, the position of the support has moved by 0.025mm/2, because the mechanical resolution of the support movement is 0.025mm. So, between the two lines there is an indeterminacy of the measurement.

Figure 6: Close up of the micrometer dial of the tool post slide hand-wheel of a conventional lathe. Each line of the micrometer dial changes the tool post slide position by 0.025mm. Note that in any position between two lines, the movement of the tool post slide could not be defined.

Finally, the *speed* of a gear train output, defines the resolution of the measurement i.e. the accuracy of the pointer (gearing output) regarding the presented result (output information). The output of *Low Speed* pointers represents a large capacity information, but in a low resolution of the calculation. Therefore, the two spiral pointers (Metonic and especially Saros), are indicators for information rather than for precise calculations based on geometry, as are the Lunar Disc and the Golden sphere. According to **Table II** the mean ratio of the two speeds of the Antikythera Mechanism is about 1/55.

A significant notation, arising from the results of **Table II**, is that the eclipse events on the Antikythera Mechanism, are presented only by the Saros pointer, a *low speed* output, i.e. a low resolution calculation, without results based on the geometry. Moreover, the Saros pointer, is a long length pointer (≈82mm), with thickness of about 2mm (or less) (Anastasiou et al., 2014) and it is a delicate and mechanically sensitive part.

Although the geometrical aligning of the Lunar Disc and the Golden sphere, is directly correlated to the Metonic spiral information, this specific geometrical aligning, only offers a probability and not a certainty (a precise calculation) for an eclipse event.

Moreover, because of its low resolution, the Saros spiral is more of an "*eclipse information table*", rather than an eclipse prediction scale. Therefore, it seems that the Antikythera Mechanism lacks a high speed gear training for eclipse predictions/calculations that could present high resolution results by means of a pointer, which is exclusively based on the geometry.

Table II: *The Low and High speed gear trains and pointers of the Antikythera Mechanism. Note that all of the (gearing) cycles present Low and High resolution measurements except the Saros gearing.*

	Periods of the Antikythera Mechanism pointers	***Low Speed* gear training- Low Resolution calculation**	***High Speed* gear train- High Resolution calculation**	**Angular Ratio High Speed / Low Speed**
1	Synodic month: Lunar phase Full moon of 1^{st} day / New moon 15^{th} day of synodic month	Decorative Lunar phase little sphere on the lunar disc (6mm diameter). Black or White, no scale	Central front dial Lunar pointer: Aiming to the Golden Sphere/Opposite position to the Golden Sphere, (0°/180°)	No ratio
2	Metonic period (19^{y})	Five full turns on Metonic spiral, 1800° spiral dimension (travel ≈ 1130mm)	254 full rotations of the Lunar Disc (sidereal)= 91440°, (travel ≈ 79756mm)	91440°/1800° ≈ 50.8
3	Saros period (18^{y} 11^{d} 8^{h})	Four full turns on Saros spiral, 1440° (spiral linear dimension ≈ 1445mm)	≈ 241 full rotations of the Lunar Disc (sidereal)= 86760°, (travel ≈ 75674mm)	86760°/1440° ≈ 60.25
4	Tropical year: Golden Sphere full rotation	Metonic spiral pointer: 5 turns/19^{y} = 0.263 turns per tropical year (≈ 94°).	13.368 turns of the Lunar Disc ≈ 4812.5° (travel ≈ 3358mm), one full turn of the Golden Sphere (travel ≈ 440mm)	4812.5°/94° ≈ 51
5	Tropical year: Golden Sphere full rotation	Saros spiral pointer: 4 turns/18.03^{y} = 0.221 turns per tropical year (≈ 80°).	13.368 turns of the Lunar Disc ≈ 4812.5° (travel ≈ 3358mm), one full turn of the Golden Sphere (travel ≈ 440mm)	4812.5°\80° ≈ 60
6	Tropical year: Golden Sphere full rotation	1 quadrant of the Athletic Games scale, 90° (travel ≈ 12.5mm)	13.368 turns of the Lunar Disc ≈ 4812.5°	4812.5°/90° ≈ 53
7	Synodic Month on Metonic spiral	Each cell on Metonic spiral ≈ 7.6°/cell, (travel ≈ 7mm)	Re-aiming of the Lunar pointer to the Golden Sphere, after one turn ≈ 389.1° (travel ≈ 2715mm)	389.1°/7.6° ≈ 51
8	Synodic Month on Saros spiral	Each cell on Saros spiral ≈ 6.4°/cell, (travel ≈ 6.5mm)	Re-aiming of the Lunar pointer to the Golden Sphere, after one turn ≈ 389.1° (travel ≈ 2715mm)	389.1°\6.4° ≈ 60
9	Solar/Lunar Eclipse prediction	Probable Saros spiral cell (synodic month)		

		≈ 6.4°/cell (travel ≈ 6.5mm)	**???**	**- - -**

The authors believe that the ancient manufacturer would not rely on the Saros pointer, a low resolution pointer and on the Saros spiral inscriptions (an information table), for the prediction of the eclipses – the most important prediction events of the Mechanism – without taking into account geometrical, high resolution calculations for these events. Because of the existence of the two different speeds on the Mechanism, the authors consider that the Antikythera Mechanism must have had an additional gear training, with an output dedicated on the eclipses prediction. This pointer should be the output of a high speed gear training, based on geometry, thus offering a high resolution calculation, so that the eclipse prediction calculation results, would be highly accurate and certain (see Chap. 7).

5. The Fragment D - description and analysis of the gear *r1*

Fragment D is an enigmatic and unplaced part of the Antikythera Mechanism. It was first noted by I. Svoronos and captured by A. Rehm in 1903, it was then misplaced and re-found in 1973 (Price 1974; Lazos 1994; Freeth and Jones 2012). Fragment D is strongly corroded/calcified in multiple thin layers, visible by naked eye. Its mechanical design information cannot be clearly detected Fig. 7. Fragment D is not correlated with the rest parts of the Mechanism.

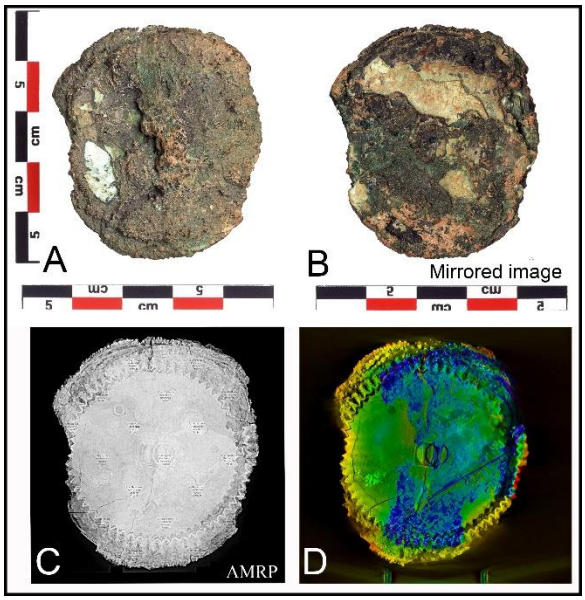

Figure 7: A) The front (original image) and B) back (mirrored image) visual photographs of Fragment D (Credits: National Archaeological Museum, Athens, K. Xenikakis, Copyright Hellenic Ministry of Culture & Sports/Archaeological Receipts Fund). C) Same scale AMRP corresponding radiography.

D), Composite AMRP selected tomographies in pseudo colors, processed by the authors. The difference of the hole and the pin positions, as a result of the displaced parts after the breakage of the gear shaft, is clearly visible.

By studying the AMRP Tomographies (AMRP, www.antikythera-mechanism.gr), Fragment D consists by three parts (Freeth and Jones 2012).

The first part is a partially preserved Circular plate, with diameter 43mm (thickness about 1mm, authors' measurements), with a square central hole. On this Circular plate, three perpendicular pins placed symmetrically by 120° relative to the center, are clearly detected Fig. 8. By observing the preserved circular perimeter shape, it arises that this plate could not be a gear. On this plate surface area, there is no detection of any engraved line or subdivisions, that could lead someone to hypothesize that the plate was a measuring scale.

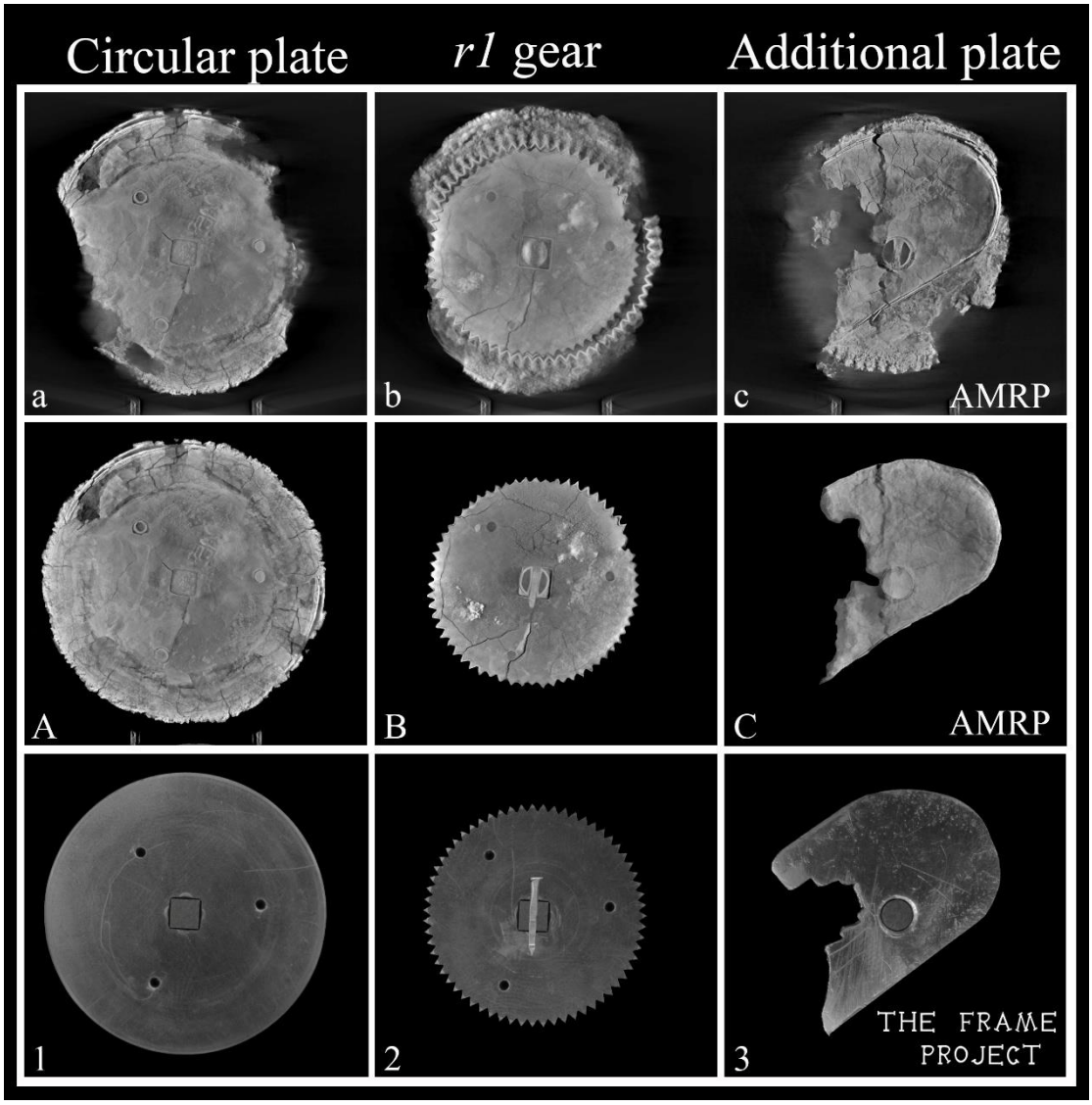

Figure 8: Selected AMRP tomographies of a) the Circular plate, b) the gear r1, c) the Additional plate. A) the digital reconstruction of the Circular plate tomography, using well preserved areas of the plate, B) the digital "cleaning" of r1 gear, from its corrosion and the deposits, in order to make its

mechanical characteristics, better visible. The stabilizing pin has also been placed on its correct position, C) the digital "cleaning" of the Additional plate, from its corrosion and the deposits. Also, the circular hole of the plate and the circular cross section of the gear shaft (probably the end of the shaft's edge), which is placed on the circular hole of the Additional plate, are presented. AMRP tomographies were processed by the authors. 1), 2), and 3) the corresponding original bronze material reconstructions of the three parts of Fragment D, designed/constructed by the first author.

In contact to the Circular plate, the gear *r1* is clearly visible (thickness about 1.5mm) preserved in very good condition. Its radius slightly varies because of the contractional deformation and the random cracks (Voulgaris et al., 2019b), between 16.7mm-17.2mm. This gear also has a square central hole. C.Karakalos (Price 1974); Wright 2005; Freeth et al., 2006; Freeth and Jones 2012, measured 63 gear teeth (61 teeth well preserved and 2 teeth missing). Around the perimeter of the gear stacked deposits of salts, calcites and petrified silt are located, following the shape pattern of the teeth, but a large percentage of these formations have been peeled out of the teeth boundaries. On this gear, the three pins are also clearly detected Fig. 8, with which the gear is stabilized on the Circular plate (stabilizing pins have also been detected on the gears *c1*/*c2* and the *l1*/*l2*). This means that the gear *r1* and the Circular plate rotate with the same angular velocity, as one body. It seems that this Circular plate is a base for *r1* gear, increasing the stability of the gear.

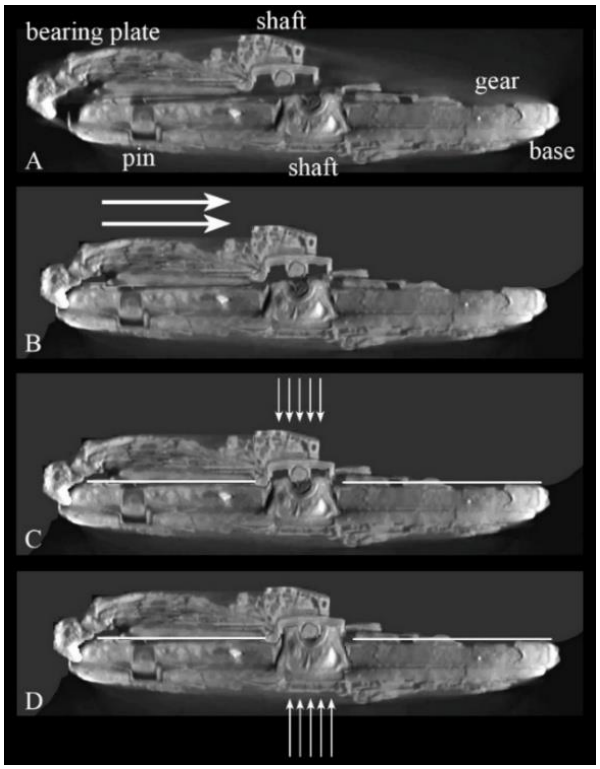

Figure 9: The four stages for the relocation on the correct position of the Additional plate and the broken r shaft. A) The present position of the Additional plate and the shaft. B) Digital relocation of these two parts, in order to align the broken shaft to the same axial direction with the main part of the

shaft (i.e. the remaining shaft on the gear). C) Relocation of the shaft and the stabilizing pin, in order for the pin to be in contact up to the gear surface (white line). By the specific position of the hole on the main part of the shaft (i.e. below the gear surface), it is evident that the main part of the shaft (which is preserved inside the gear) is also displaced or shrunk, because of the contractional deformation (Voulgaris et al., 2019b). D) A digital relocation of the main part of the shaft in perpendicular direction up to the stabilizing pin, is presented. The relocation travel is about 0.4mm-0.5mm.

Close to the gear surface and perpendicular to the gear shaft, a hole can be detected, in which the stabilizing pin of the gear was adapted. On this area, the shaft is broken. Above this hole, the AMRP tomographies reveal the stabilizing pin, the rest part of the broken axis and a strange shape piece, the Additional plate. These pieces have been displaced from their original position, as is evident by the difference in position of the corresponding formations (gear shaft, hole and pin) Fig. 8,9. The Additional plate (thickness about 1mm-1.5mm) is partially preserved in a particular shape, Fig. 8,9. Visible on the Additional plate is a circular hole, in which the broken and displaced circular axis, is adapted.

The extended study of the AMRP Tomographies (original and also processed by the authors), does not reveal any proof for the existence of the three pins on the Additional plate, that could lead someone to consider that the Additional plate was fixed/stabilized on the gear *r1*. The clearly visible edges of the three pins are detected only between the Circular plate and the gear Fig. 9. Moreover, one of the three pins is totally out of the boundaries of the Additional plate Fig. 10E.

Additionally, the existence of the perpendicular stabilizing pin of the shaft, between the gear and the Additional plate, prevents any contact between the surfaces of the two parts Fig. 8B, and 10C,D. Of course, before the material corrosion/calcification, the distance between *r1* gear and the Additional plate, was at least 0.9mm-1.0mm, which is the thickness of the perpendicular stabilizing pin. Therefore, the Additional plate is not in contact to the *r1* gear and is totally independent from it.

Inside the circular hole of the Additional plate, the broken part of the gear shaft is also preserved, which at this point has a circular cross section Fig. 8,10. The circular cross section design means that during the rotation of the *r1* gear and its shaft/axis, the Additional plate does not rotate and it is totally independent to the gear/shaft rotation.

The authors cannot find any other realistic mechanical operation for this Additional Plate, except that it was a simple oblong plate-*artistically curved* by one side (of which today only this part remains), acting as one out of two bearing points-plates for *r1* shaft (see Chap. 7

and Fig. 15): most of the Mechanism axes/shafts, are supported on two opposite points-plates. For example, the preserved shafts *f*, *g*, *h*, *i*, are supported between two parallel plates Middle and Back (this is also mandatory for the lost shafts *m*, *n* and *o*) and the *d* shaft, between the Middle plate and the Ω-*shape Retention bar* (Voulgaris et al., 2018b).

In Efstathiou et al., 2011; Anastasiou 2014; Basiakoulis et al., 2017; Seiradakis 2018 (slides 224-238), the Additional Plate is represented as fixed on the gear *r1* and rotating with the same angular velocity. It is also suggested that this plate acts as a cam leading to the calculation of the Equation of Time. This consideration does not agree with the AMRP tomographies and the observations presented in this paper. Moreover, this suggested design, has lots of additional real disadvantages, related to the suggested position of the gear *r1*, its stabilization, its operation, the way the results are displayed and the nature of these results.

It is obvious that if the ancient manufacturer wanted to make the Additional plate to rotate with the same angular velocity to the *s1* gear, he should have at least made the hole of the Additional plate and also the corresponding cross section of the *r* shaft, square. Moreover, the stabilizing pin between the *r1* gear and the Additional plate, prevents any immobilization of the Additional plate on the gear, even if it had square cross section.

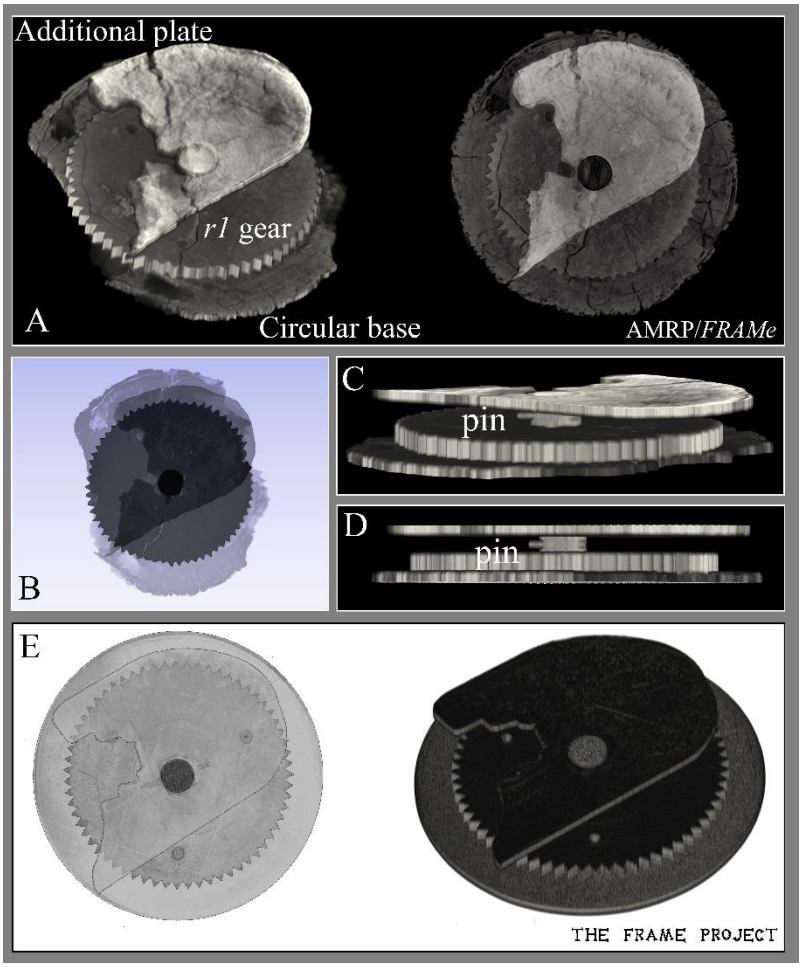

Figure 10: A) A 3D representation using the 3D Slicer software (Fedorov et al., 2012), of the digitally reconstructed and "cleaned" AMRP tomographies of Fragment D, processed by the authors. B) The Fragment D represented in transparent layers. C and D) Two side views, in order to make the pin position visible. E) Left, the transparent and Right, the 3D representation of the "artificial radiographies" of the three assembled original bronze reconstructed parts, using the 3D Slicer software. Photos and processed images, by the first author.

The existence and the specific position of the perpendicular stabilizing pin, leads to the conclusion that the pin was adapted in order to stabilized the gear on the specific position. It also results that gear shaft, was extended beyond the side of the Circular plate-base (today is missing), as is also observed on most of the preserved gear shafts of the Mechanism (e.g. shafts *g*, *h*, *i*).

The engraved letters "*ME*" are detected on three different places on the Fragment D. Engraved letters have also been detected on two other gears of the Mechanism, on *m1* (letter *H*) and on *b1* (letter *N*). These letters could be the assembly numbering of the parts (?), or it could be a more secret scenario, e.g. the manufacturer could have written his name or a phrase spread out on several parts of the Mechanism (?).

6. The engaged gears *b1-a1*, the output on the *a* shaft

The *b1* gear is the largest gear of the Mechanism (Freeth et al., 2006). In contrast to *e3* gear (the second larger), which is made by one piece of circular plate, the *b1* gear consists of several assembled parts, which form four radial bars and a ring with teeth. The rest surface area of the gear does not have any bronze material. The absence of the material resulted to the irregular and relative strong, three dimensional deformation (shrinkage) of the *b1* gear, mostly by the long-time stand still of the Mechanism on the sea bottom and its abrupt dehydration after its retraction from the sea (Voulgaris et al., 2019b).

Teeth number measurements of *b1* gear (in its present condition) were made by C.Karakalos (223-226 teeth), D.S.Price (225 teeth), M.T.Wright (216-231 teeth) and Freeth et al., 2006, (223-224 teeth). An additional problem for the precise measurement of the teeth number, is the difficulty for the detection of the true teeth boundaries and tip position: many of the preserved gear teeth are filled with deposits (salts, calcites etc., as also observed on the *r1* gear) that are following the shape of the gear perimeter, but at the same time they are altering or covering or erasing, the triangular shape of the teeth Fig. 13. In some areas, the teeth are worn out or destroyed or totally missing. Moreover, the *b1* gear radius varies about ±1.1mm (Freeth et al., 2006, see also graph of Fig. 11).

The calculation of the total teeth number is achieved by first measuring the preserved teeth and the corresponding epicenter angle (of course on their present condition and position) and afterwards according to the equation: total gear teeth = (teeth number/corresponding epicenter angle) X 360°. Obviously, the corresponding epicenter angle is not the original-true angle, because of the gear's 3D (contractional) deformation (Voulgaris et al., 2019b). The epicenter angle measured between the teeth tips on a part with shorter radius (i.e. shorter perimeter), results to a smaller calculated gear teeth number (see Fig. 11). Obviously, the calculation of the mean value of the authors' measurements was avoided, because the statistic average values of the measurements does not approach the initial/original teeth position, as most (or all) of the teeth positions are displaced by the deformation. All of these, make difficult the precise detection of the true teeth boundaries and tip position.

Of course, before the contractional deformation of the Mechanism, the original radius of the gear was larger. The authors' measurement of the gear teeth number is in the range of 219-225 teeth (see the graphs of Fig. 11). This, leads to the conclusion that the original teeth number of the (bronze un-corroded/non-deformed) gear, must have been closer to the upper number of this measurement.

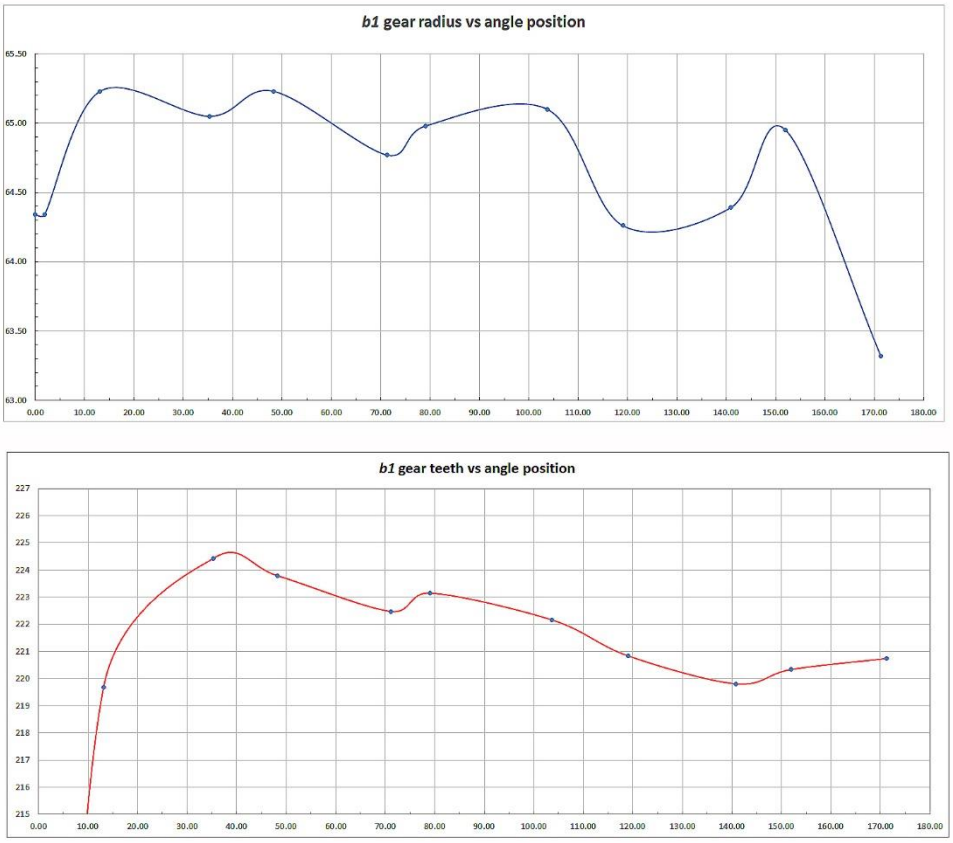

Figure 11: A) The graph of the b1 gear radius vs angle position. Because the geometrical/mechanical centers of the two axes b_{in} and b_{out}, differ by about 0.4mm (as a result of the contractional deformation), the geometrical center of b1 gear central circular hole, was selected as the center for the radius and epicenter angle measurements. B) The graph of the calculated gear teeth number of b1 gear vs angle position. This graph more or less has similarities in the monotonicity to the above graph, as a result of the radius variation. Authors measurements.

The contrate gear/shaft *a1* was ceremonially considered as the "input" of the Mechanism. Based on the observations of Voulgaris et al. 2018b, for several, very important mechanical and operational reasons, the most probable input is the Lunar Disc. This observation creates an additional output of the Mechanism with unknown operation, the shaft of *a1* gear.

Gear *a1* with (definite) 48 teeth (Freeth et al., 2006), is located on the right side of the Mechanism and is engaged with *b1* gear Fig. 12. Gear *a1* and its shaft, rotate in perpendicular direction to the rest gearing trains. The gear has a rectangular central hole, in which the poorly preserved rectangular shaft is adapted. A central conical hole, a result of the shaft material processing during the construction by an ancient lathe (Voulgaris et al., 2018b and 2019a), is visible by naked eye. In AMRP tomographies, a relatively thick pin with oblong cross section, perpendicular to the gear *a1*, is detected, Fig. 12F,G. This pin differs

than the usual stabilizing pins, and it seems that it is an immobilizing pin, in order to fix a cylindrical bronze material (gear) to its shaft, probably before the material processing.

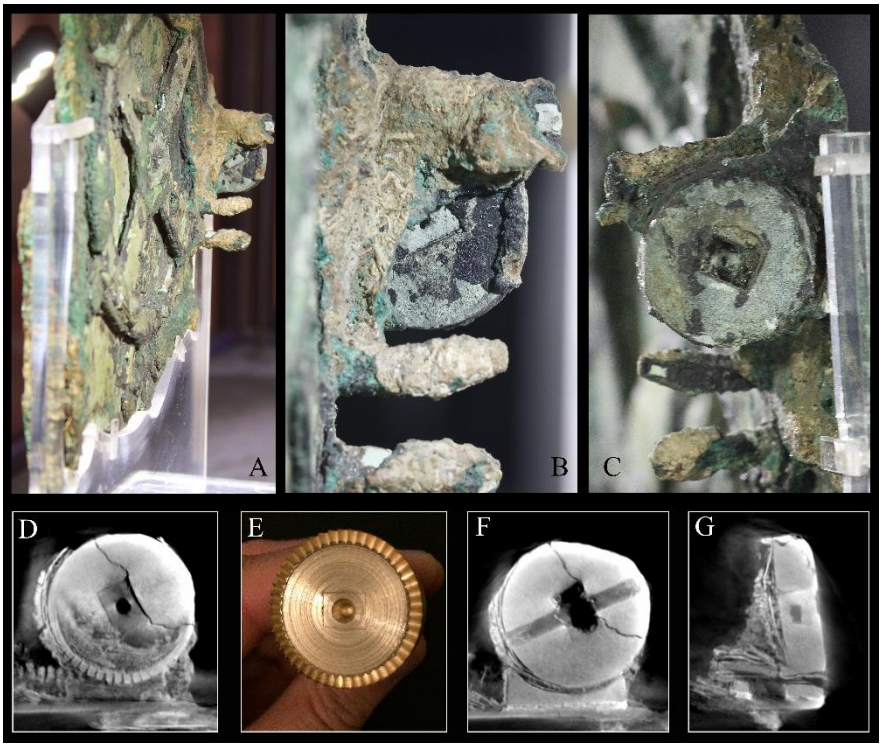

Figure 12: A) The position of the contrate gear a1 relative to the gear b1. B) Front face close-up of the contrate gear a1. The (conical) central hole on the shaft is slightly visible, C) Back face close-up of the contrate gear a1 (Credits: National Archaeological Museum, Athens, A. Voulgaris-Copyright Hellenic Ministry of Culture & Sports/Archaeological Receipts Fund Photos), D) AMRP right side view tomography of the gear a1. Some of the gear teeth are visible and also the gear shaft with rectangular cross section and the (conical) central hole of the shaft, E) Bronze reconstruction of the a1 contrate gear, by the first author. F) The large pin, which immobilizes the a1 gear to its shaft, and the driver/nest of the gear, are clearly visible, G) AMRP top side view tomography of the gear a1. The rectangular cross section of the large and thick immobilizing pin is visible.

Between the *a1* gear and the Middle plate, a part is detected which is stabilized on the Middle plate by the use of an adhesive material (an alloy of and tin and lead, Voulgaris et al., 2018c). This part acts as a driver (nest) for the *a1* gear, in order to avoid the (probable) precession or displacement during its rotation, causing its disengagement with the *b1* gear Fig 12F.

The gear *b1* is stabilized on the gear *b2* by four pins and rotates with the same angular velocity (Freeth et al., 2006; Voulgaris et al., 2019b revised gearing scheme). Gear *b2* belongs to the main gearing of the Mechanism and its rotation represents the tropical year on the Mechanism. The larger *b1* gear does not have any correlation to the main gearing of

the Mechanism and regardless of its teeth number or even if it did not exist, it would not affect the main gearing sequence of the Mechanism. Therefore, this gear was adapted by the ancient manufacturer in order to introduce a new additional gearing, which started its movement by the engagement of the *a1* contrate gear with *b1* gear. The contrate gear transmits the movement in perpendicular direction to the rest gearing axes direction. The presence of the *a1* contrate gear, leads to the conclusion that the ancient manufacturer wanted to extent the gearing in perpendicular direction, in order to be continued to the right side of the Mechanism. If he wanted the new gearing to continue the rotation on the same direction, he could use a simple gear with 48 teeth instead of a contrate gear.

In contrast to most of the other gearing trains, which are engaged in reducing/dividing ratios, the *a1* gear/shaft rotation originates from a multiplying ratio: *b1*/*a1* ≈ 4.6 rotations of *a* shaft per one rotation of *b1*(*b2*) gear-tropical year.

7. Adapting the Fragment D on the Antikythera Mechanism

From Chapter 4 results that there is no *High Speed* (*High Resolution*) gearing for the eclipse prediction based on geometrical calculations. At the same time, an unknown output of the Mechanism and an unplaced gear exists. Following is a presentation of the thinking, the design, the gearing mathematical calculations, the use and the results of a new gearing, suggested by the authors, in order to achieve precise eclipse predictions based on geometrical calculations.

A new gearing can be introduced, in order to represent the second necessary parameter for the eclipse prediction: a gearing representing the draconic cycle - the fourth lunar cycle, is needed (see chap. 3). The output of the draconic gearing is a draconic pointer. This gearing train must be a *High Speed* (*High Resolution*), in order to extract results based on geometrical calculations.

Therefore, the draconic gearing must be adapted in a position where the gears' speed is high and at the same time, the candidate position must allow the adaptation of the additional mechanical parts. A proper position for the new gear training, is difficult to be placed close to the Lunar Disc (which easily presented the synodic/sidereal rotation), because the ratio draconic month/synodic month, cannot be precisely represented using small numbers, i.e. via a train of 2-3 engaged gears/also in small diameters i.e. small teeth number (see **Table I**).

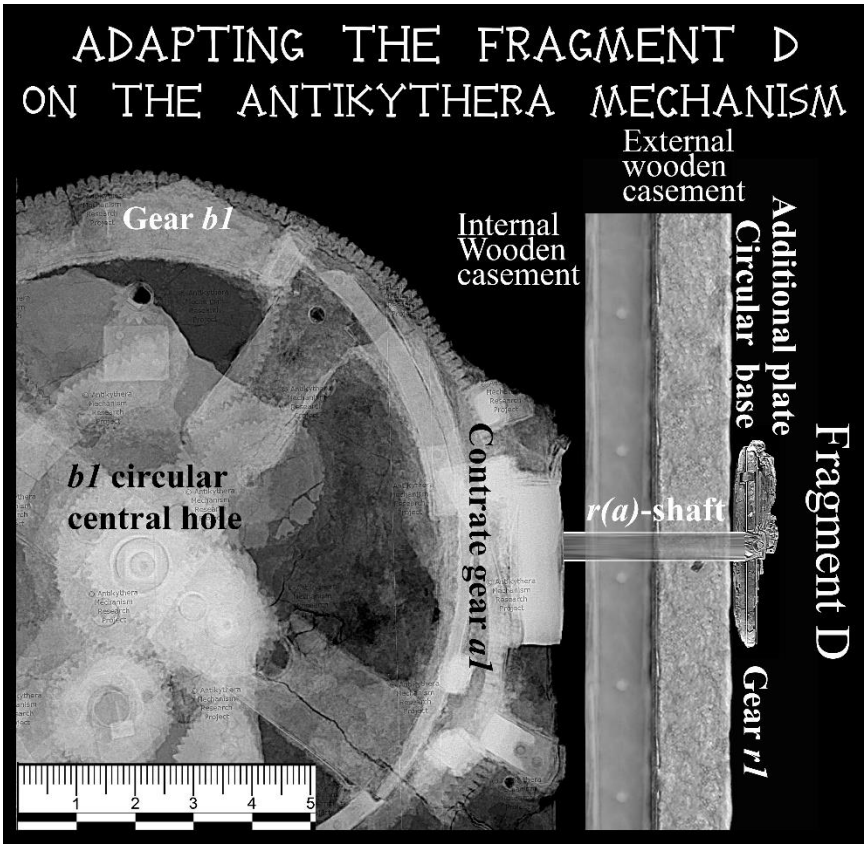

Figure 13: Same scale, digital placement of Fragment D on Fragment A, via the r(a)-shaft (partially preserved today), which is also the common shaft of the a1 contrate gear. The Circular (Bearing) base of Fragment D is on the right side of the External Wooden Decorative casement (Voulgaris et al., 2019b). Fragment D is presented, according to the digital restoration/correct placement of the displaced parts, see Fig. 9,10. The AMRP radiography (Fragment A) and tomography (Fragment D) were processed by the authors.

A proper position for this new-draconic gearing can be achieved on the *a* shaft-output, which starts by the engaged gears *b1-a1*. On the other edge of the *a* shaft, the *r1* gear is adapted Fig. 13. The mechanical design and the dimensions of the *a* shaft, allows the adaptation of *r* shaft/*r1* gear. A hypothetical gear *s1,* engaged to *r1* gear is needed for the output of the draconic gearing train. The draconic pointer is adapted on the *s* shaft Fig. 13,14.

One full rotation of the draconic pointer corresponded to one draconic month. The measuring scale of the draconic pointer depicts the Ascending and Descending Node-points. Two simple pins in up/down position, anti-diametrically placed and stabilized on the External Wooden decorative casement (Voulgaris et al., 2019b), represent the two Nodes, one gold pin for the Ascending Node and one silver pin for the Descending Node. On either side of each Node-pin there must also be an arc shaped bronze strip, depicting the max limits of the

Zone of Eclipses, ±17° for each Node Fig. 14. A draconic month is completed, whenever the draconic pointer returns to the same Node-pin, after one rotation.

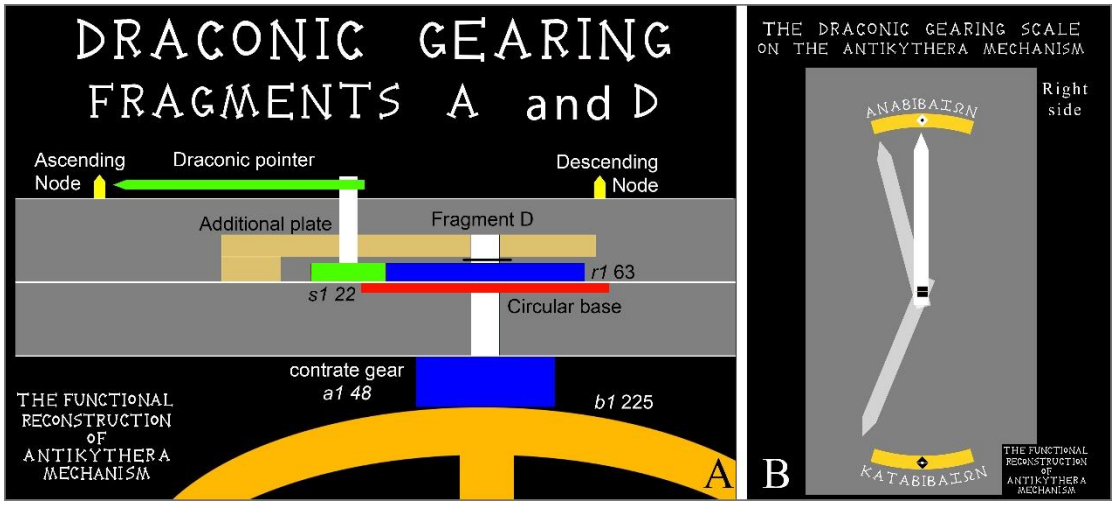

Figure 14: A, The position of the mechanical parts and the gear teeth number of the draconic gearing. B, the draconic scale: the draconic pointer, the Ascending (ΑΝΑΒΙΒΑΖΩΝ) and the Descending (ΚΑΤΑΒΙΒΑΖΩΝ) pin-Nodes and the two eclipse limits, are depicted. When the Draconic pointer aims inside the Zone of eclipses limit, a solar or lunar eclipse will occur (depending on the relative position of the Lunar disc and the Golden Sphere-Sun). If the pointer aims outside the Zone of Eclipses limit, there will be no eclipse.

For the gear teeth calculations, the lunar cycles of Saros period (**Table I**) were selected, as the most proper period for the eclipse prediction.

One Saros period of 223 synodic months = 242 draconic months. Therefore, on the Antikythera Mechanism, 242 full rotations of the draconic pointer are equal to 223 synodic rotations of the Lunar Disc (i), and also from the Metonic gearing 235 synodic rotations = 254 sidereal rotations or 1 synodic rotation of the Lunar Disc Input = 254/235 sidereal rotations (ii).

Therefore, 242 draconic rotations = 223 * 254/235 sidereal rotations (iii). Applying this equation on the Antikythera Mechanism gearing:

[223 * (254/235)] * (*b3/e1*) * (*e6/k2*) * (*k1/e5*) * (*e2/d2*) * (*d1/c2*) * (*c1/b2*) * {(*b1/a1*) * (*r1/s1*)} = 242 rotations of draconic pointer (iv), therefore

(*b1/a1*) * (*r1/s1*) = 13.42223271 (v).

For *a1* = 48 teeth (definite) and *r1* = 63 teeth (definite), the equation (*v*) becomes

b1/*s1* = 10.22646302 (vi).

For a gear teeth number of *b1* = 225 (see Chap. 6), the equation (vi) results

s1 = 22.00174 teeth, rounded to 22 teeth for the gear *s1*.

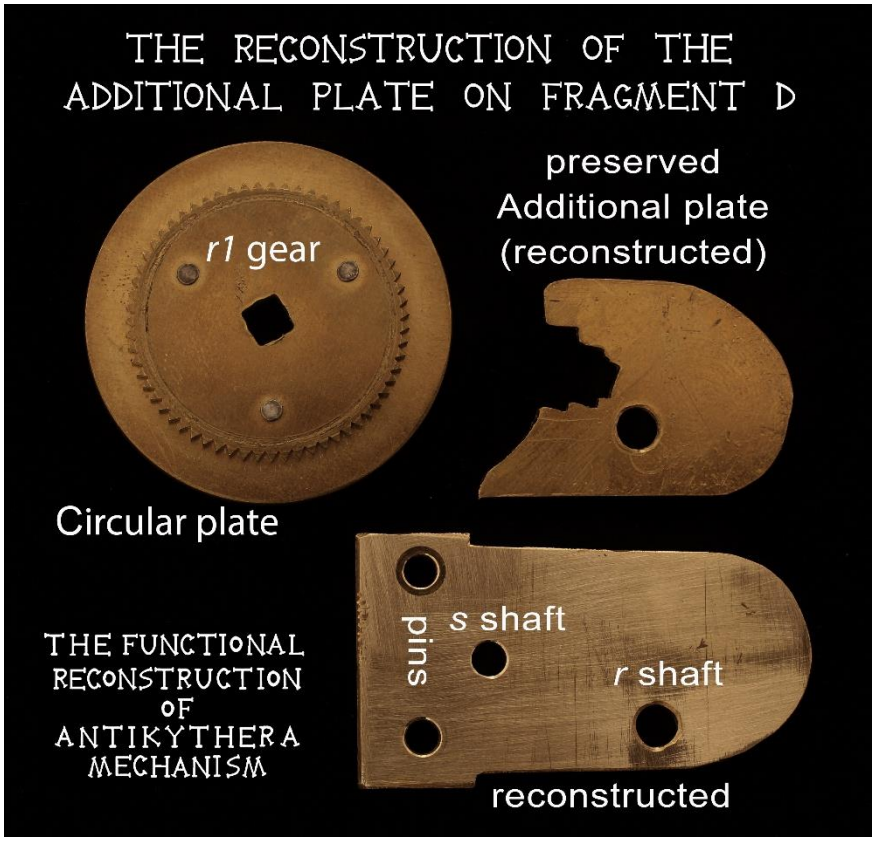

Figure 15: The bronze reconstruction of the Additional (bearing) plate on Fragment D, taking into account Figures 14,16. The holes for the r and s shafts are presented. The two holes on the left, were made for stabilizing the Additional plate on the Internal Wooden casement, by the use of two pins. Reconstructed parts by the first author.

From the above calculations, it results that for one rotation of *b1* gear (one metonic tropical year of 365.2631579^{d}), the draconic pointer rotates 13.42329545 times (draconic months), so 365.2631579^{d}/13.42329545 = 27.21113896^{d}/draconic month, instead of 27.21218683^{d} (resulting from the true values of Saros cycle presented on **Table I**). The gearing exhibits a phase difference-error of -0.00104787^{d}/1 draconic pointer rotation, i.e. about -1.5 min/draconic month. Of course, such an error is too small compared to the mechanical errors of the Mechanism gearing (Edmunds 2011).

Table IV: *Continuing from* **Table I***: the Low and High speed pointers for the Antikythera Mechanism eclipse prediction, introducing the draconic gearing on the Mechanism.*

Periods of the Antikythera Mechanism pointer	***Low Speed* gear training-Low Resolution calculation**	**Draconic *High Speed* gear train-High Resolution calculation**	**Angular Ratio High Res / Low Res**
Eclipses calculation/prediction	4 turns of Saros pointer/ 1 Saros cycle	242 turns of Draconic pointer /1 Saros cycle	87120°/1440° = 60.5

7.2 The "*scenic*" operation of the draconic gearing on the Antikythera Mechanism

By introducing the draconic gearing on the Antikythera Mechanism, the operation of the high resolution eclipse prediction based on the geometry, is achieved. The specific position of the draconic pointer on the right side of the Mechanism Fig. 16, has also a special *scenic operation*: as the user rotates the Lunar Disc, when the lunar pointer aligns with the Golden Sphere-Sun i.e. New Moon phase (*corresp.* in opposite direction-Full Moon), he can also easily observe at the right side of the Mechanism, to see if the draconic pointer is located inside one of the two arc limits-Zone of Eclipses (bronze strip). If so, then he knows for sure that a solar (*corresp.* lunar) eclipse will occur. Afterwards, he turns the Mechanism to the other side (Back plate) and by observing the cell that the Saros pointer aims, he can read the eclipse information for the time of the eclipse event and also the metonic month in which the eclipse occurs. Of course, if the draconic pointer aims anywhere out of the limits of two arc-Zone of Eclipses, it is totally sure that the corresponding Saros cell, is empty (see Fig. 4).

It is possible that the ancient manufacturer engraved the eclipse events sequence (glyphs) on the corresponding cells of the Saros spiral, by observing the relative position of the Lunar Disc pointer to the Golden sphere-Sun and at the same time the position of the draconic pointer relative to the Zone of Eclipses limits, while rotating the Lunar Disc-Input of the Mechanism.

Regarding the letters "*ΜΕ*", referred three times on the Fragment D parts, they could also be considered that they are the headings of the words "*ΜΗΝ ΕΚΛΕΙΠΤΙΚΟΣ*" or "*ΜΗΝ ΕΓΛΕΙΠΤΙΚΟΣ*" (Ecliptic Month), which is related to the three draconic gearing parts. The Ecliptic (ΕΚΛΕΙΠΤΙΚΗ) is referred on the Mechanism Back cover inscriptions as "*ΧΡ(ΟΝΟΙ)…. ΕΓΛΕΙΠΤΙΚΟΙ*" (*times of eclipses*) Bitsakis and Jones 2016.

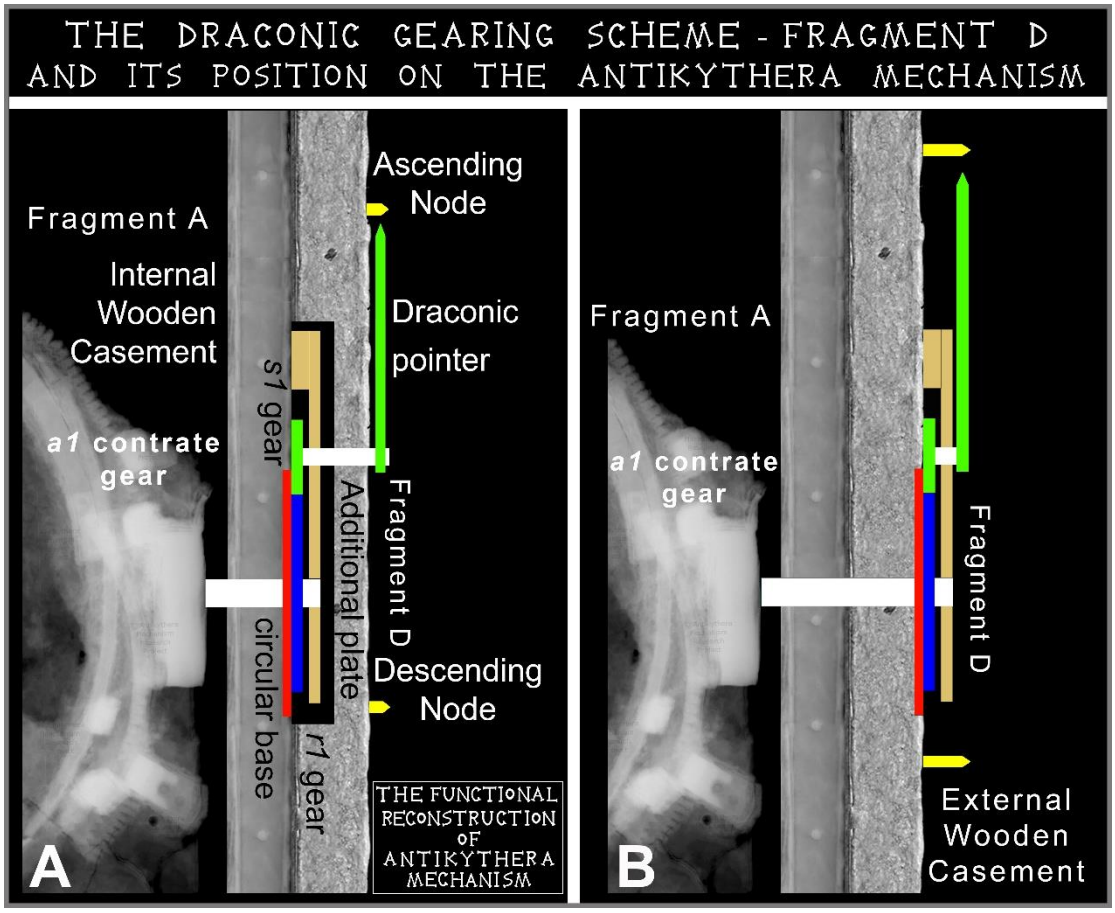

Figure 16: The draconic gearing scheme-Fragment D, positioned on the right side of the Antikythera Mechanism. The r(a) shaft, the Circular base, the (hypothetical) gear s1, the draconic pointer and the two Node-pins, are presented. The Circular plate enhances the stabilization of the a1 and the r1 gears. A) The first gearing scheme design, with the gearing parts adapted on the Internal Wooden Casement (Voulgaris et al., 2019b). B) The same design, adapted on the External Wooden Decorative Casement. This design has the disadvantage that the mechanical parts of the gearing are located outside the boundaries of the Mechanism. The r shaft penetrates the Internal Wooden Casement (design A) and also the External Wooden casement (design B).

7.3 The variable velocity of the Moon - *pin&slot* gearing motion, visible on the draconic pointer

From Voulgaris et al., 2018b, it is obvious that the variable velocity achieved by the gears *k2-k1* and transferred on the following gearing sequence, is not visible to the naked eye by observing any part of the Mechanism, because the gears' rotation is in reduced angular velocity (slower motion) than the input/*pin&slot* gearing, and therefore the variability in the velocity is also reduced.

On the other side, the rotation period of the draconic output-pointer, is about equal to the Lunar Disc sidereal rotation period: from the equations (*a*) and (*b*) it results that 1 Saros = 242 draconic cycles ≈ 241.029 sidereal cycles i.e. 1 sidereal rotation (360°) of the Lunar Disc ≈ 1.004028 draconic rotations (≈ 361.45°) (Voulgaris et al., 2018b), i.e. the draconic pointer rotates a bit faster than the Lunar Disc pointer Fig. 17.

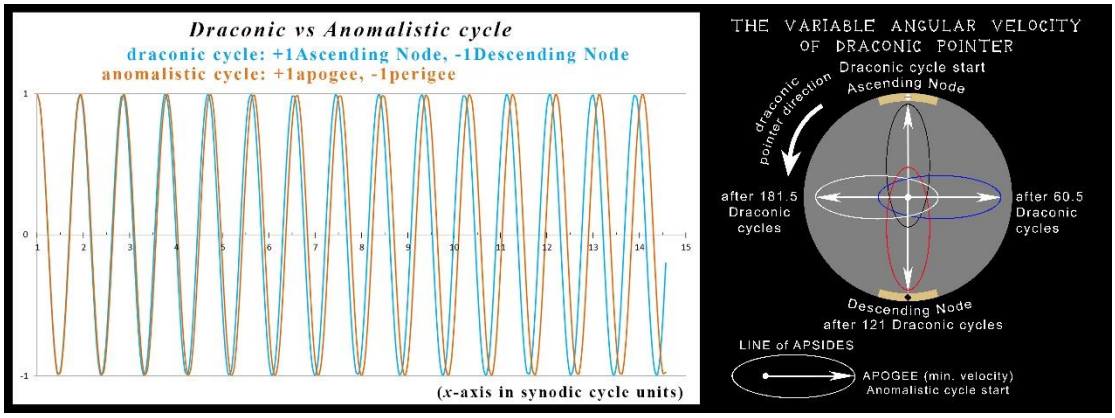

Figure 17: Left, harmonic graph of the draconic and anomalistic cycles, assuming that they start on the same phase (draconic in Ascending Node, anomalistic in apogee) and during the New Moon phase. The units of the x-axis (time), are in synodic cycles. Right, the white arrow represents the position of the Line of Apsides relative to the Nodes, which changes its position during the rotation of the draconic pointer (not depicted in the scheme). The draconic cycle starts with the arrow head pointing to the Ascending Node (Anomalistic month start - apogee), so that the moon crosses the Node with the minimum velocity. After 121 Draconic cycles (half Saros-Sar), the draconic pointer crosses the Ascending Node with the maximum velocity-perigee. On the 60.5th and also on the 181.5th draconic cycle, i.e. when the draconic pointer aims to the Descending Node, the pointer crosses the two Nodes with about its mean angular velocity.

On the Saros cycle, 242 draconic months are also equal to ≈239 anomalistic cycles i.e. 1 anomalistic month (from apogee to the next apogee) ≈1.01255 draconic months. This means that the Line of Apsides (the line connecting the points of min and max lunar velocity), delays on each draconic rotation, i.e. rotates in opposite direction relative to the Line of Nodes Fig. 17.

On the Antikythera Mechanism, this change is visible on the draconic pointer. The draconic pointer rotation presents a variable angular velocity and the max-min velocities (Line of Apsides) change their position relative to the Nodes. The imaginary Line of Apsides, slowly rotates in opposite direction (CW) to the direction of the draconic pointer rotation (CCW). This means that the draconic pointer returns to the same Node-pin, each time by a different velocity, as it also happens every time the moon approaches a Node Fig. 17, see also Fig. 2.

8. Epilogue

The Fragment D/gear *r1* was an unplaced part of the Antikythera Mechanism, with unknown operation. In this work, an ideal position and operation for this enigmatic part is presented, taking into account the present condition and the preserved parts of the Antikythera Mechanism. According to the authors' opinion, the existence of the draconic gearing offers the necessary precise eclipse prediction/calculation of the Mechanism. The authors tried to correlate, by using the minimum hypotheses required, an unplaced gear with an unknown gear training output of the Mechanism, without adding any too hypothetical or theoretical parts and scenarios. For this attempt, the dimensions of the preserved parts, were taken into account. The simple design/construction of the draconic gearing, includes the use of the three existing gears (*b1*, *a1*, *r1*) and also a new gear (*s1*). No additional, hypothetical complex parts and engraved scale, was needed.

This additional gearing train improves the efficiency of the instrument, which can now perform precise eclipse predictions/calculations. The adaptation of the draconic gearing/cycle on the Antikythera Mechanism, presents a complete representation of the four lunar motions that were well-known and studied in the Hellenistic era. The authors strongly believe that the ancient manufacturer of the Antikythera Mechanism, took into account the four integrated lunar motions in order to represent the celestial Cosmos on his creation.

Summarizing:

1) A realistic and relevant to the Antikythera Mechanism operation for the unknown *a1* output, was found,

2) The multiplying rotation of the *a1* gear, leads to a gear train output a few times shorter in rotation than the tropical gear,

3) A mechanically accepted position and role for the unplaced gear *r1*, was detected,

4) The existence of the two other parts of Fragment D was justified,

5) The mathematical calculations of the draconic gearing are highly accurate,

6) There is adequate space for the draconic training adaptation at the right side of the Mechanism and this specific position assists the Mechanism user during the operation,

7) The teeth number of *b1* gear was specified,

8) The existence of the specific high speed gear training, offers the geometrical calculations needed for the eclipse events prediction/high resolution calculation of the Antikythera Mechanism, improving the accuracy of the eclipse predictions,

9) The addition of the draconic gearing on the Mechanism, introduces the two mandatory lunar cycles for the eclipse prediction,

10) The invisible to the naked eye, variable angular velocity produced by the gears *k2*/*k1*/ (adapted on the *e5* gear), becomes visible on the draconic pointer rotation,

11) Finally, by introducing the draconic gearing on the Antikythera Mechanism, the incorporation on the Antikythera Mechanism gearing of the four, well-studied in antiquity, interrelated lunar motions, is achieved.

Although someone should be skeptical and wary when introducing new hypotheses regarding the Antikythera Mechanism, the authors believe there is a large number of logical reasons justifying the existence of this new operation/gearing. At the same time, they cannot find any mechanical or malfunctioning or non-correlation or teleology reason, in order to doubt or reject this new gearing.

The main conclusion arising from this work, is that the ancient manufacturer found a way to engage the four main lunar motions that were recorded, well studied and extensively used, during the time of the Antikythera Mechanism construction.

Acknowledgements

We are very grateful to the AMRP for the license and permission to use the X-ray CT images and radiographs, which were captured via equipment loaned by X-Tek System, Ltd. (now owned by Nikon Metrology). Thanks are due to the National Archaeological Museum of Athens, Greece for permission to photograph and study the Antikythera Mechanism fragments. We would also like to thank Prof. T. Economou of Fermi Institute-University of Chicago, USA, for his suggestions concerning X-Ray CTs.

Bibliography

- Anastasiou M., Seiradakis J.H., Evans J.C., Drougou S., Efstathiou K., 2013. The Astronomical Events of the Parapegma of the Antikythera Mechanism. *Journal for the History of Astronomy,* 44(2), pp. 173– 86.

- Anastasiou M., 2014. Thesis, Chap. 7, page 119, in Greek, http://ikee.lib.auth.gr/record/135226/files/GRI-2014-13217.pdf .

- Anastasiou M., Seiradakis J.H., Carman C.C. and Efstathiou K., 2014. The Antikythera Mechanism: The Construction of the Metonic Pointer and the Back Dial Spirals. *Journal for the History of Astronomy*, 45, pp. 418–41.

- Antikythera Mechanism Research Project, http://www.antikythera-mechanism.gr

- Barbieri C., 2017. Fundamentals of Astronomy. CRC Press, Chapman & Hall, Florida.

- Basiakoulis A., Efstathiou M., Efstathiou K., Anastasiou M., Seiradakis J.H., 2017. Ancient Technology and the Correction of the Time Shown by the Sun watches, Proceedings of the 6th International Conference on Manufacturing Engineering "ICMEN". 6th International Conference on Manufacturing Engineering "ICMEN". Thessaloniki, Greece, http://www.academy.edu.gr/Antikythera-Digital-Book-Files/0A_The%20Antikythera%20Mechanism_S.pdf , on pages 259–280.

- van den Bergh G., 1955. Periodicity and Variation of Solar (and Lunar) Eclipses. Tjeenk Willink and Haarlem, Netherlands.

- Bowen A.C. and Goldstein B.R., 1988. Meton of Athens and Astronomy in the Late Fifth Century B.C. In: Leichty E., de J. Ellis M., Gerardi P. (eds.), *A Scientific Humanist: Studies in Memory of Abraham Sachs* (Philadelphia), pp. 39–81.

- Brown C., 1931. The Eclipse in China, *Popular Astronomy*, 39(10).

- Carman C.C. and M. Di Cocco, 2016. The Moon Phase Anomaly in the Antikythera Mechanism, *ISAW Papers*, 11, http://dlib.nyu.edu/awdl/isaw/isaw-papers/11/

- Edmunds M.G., 2011. An Initial Assessment of the Accuracy of the Gear Trains in the Antikythera Mechanism, *Journal for the History of Astronomy*, 42, pp. 307–20.

- Efstathiou K., Basiakoulis A., Efstathiou M., Anastasiou M. and Seiradakis J.H., 2011. The Equation of Time calculated by the Antikythera Mechanism. Oral presentation, 4th International Conference on Manufacturing Engineering "ICMEN", Thessaloniki, Greece, 3-5 October 2011.

- Espenak F., and Meeus J., 2008. Five Millennium Catalog of Solar Eclipses: -1999 to +3000 (2000 BCE to 3000 CE), NASA Tech. Pub. 2008-214170, NASA Goddard Space Flight Center, Greenbelt, Maryland. NASA Eclipse catalogue,

https://eclipse.gsfc.nasa.gov/SEcat5/SE1901-2000.html ,
https://eclipse.gsfc.nasa.gov/SEsearch/SEsearchmap.php?Ecl=-05840528

- Evans J., 1998. The History & Practice of Ancient Astronomy. Oxford University Press, New York; Oxford.

- Evans J., Berggren J.L., 2006. Geminos's Introduction to the Phenomena: A Translation and Study of a Hellenistic Survey of Astronomy in English. Princeton University Press, Princeton; Oxford.

- Fedorov A., Beichel R., Kalpathy-Cramer J., Finet J., Fillion-Robin J.C., Pujol S., Bauer C., Jennings D., Fennessy F., Sonka M., Buatti J., Aylward S.R., Miller J.V., Pieper S., Kikinis R., 2012). 3D Slicer as an Image Computing Platform for the Quantitative Imaging Network. *Magn Reson Imaging* 30(9), pp. 1323–1341. PMID: 22770690, https://www.slicer.org/.

- Freeth T., 2019. Revising the eclipse prediction scheme in the Antikythera mechanism. *Palgrave Communications*, 5(7), pp. 1–12.

- Freeth T., Bitsakis Y., Moussas X., Seiradakis J.H., Tselikas A., Mangou H., Zafeiropolou M., Hadland R., Bate D., Ramsey A., Allen M., Crawley A., Hockley P., Malzbender T., Gelb D., Ambrisco W. and Edmunds M.G., 2006. Decoding the Ancient Greek Astronomical Calculator Known as the Antikythera Mechanism, *Nature*, 444, pp. 587–91.

- Freeth T., Jones A., Steele J.M. and Bitsakis Y., 2008. Calendars with Olympiad Display and Eclipse Prediction on the Antikythera Mechanism. *Nature*, 454, pp. 614–7 (Supplementary Material).

- Freeth T. and Jones A., 2016. The Cosmos in the Antikythera Mechanism, *ISAW Papers*, 11, http://dlib.nyu.edu/awdl/isaw/isaw-papers/4/

- Geminus, 1880. Gemini Elementa Astronomiae. In: Manitius K. (Ed.), Leipzig, in Greek and Latin.

- Geminus, 2002. Gemini Elementa Astronomiae. In: Manitius K. (Ed.), (Leipzig, 1880), transl. E. Spandagos, in Greek, Aithra, Athens. Γέμινος, Εισαγωγή είς τα φαινόμενα του Γεμίνου του Ρόδιου σε μετάφραση Ε. Σπανδάγου, Αίθρα, Αθήνα.

- Geogebra Dynamic Mathematics software, www.geogebra.org

- Gourtsoyannis E., 2010. Hipparchus vs. Ptolemy and the Antikythera Mechanism: Pin–Slot Device Models Lunar Motions, *Advances in Space Research*, 46, pp. 540–4.

- Hannah R., 2001. The Moon, the Sun and the Stars: Counting the Days and the Years. In: McCready S. (ed.), The Discovery of Time. MQ Publications, London, pp. 56–99.

- Hannah R., 2013. Greek Government and the Organization of Time. In Beck H. (ed.), Companion to Ancient Greek Government, Blackwell, Oxford, pp. 349–65.

- Hecht E., 2017. Optics. Pearson Education, Incorporated, 5th Ed., p.714.

- Herodotus, 1998. The Histories, Book 1, 73-74, translation R. Waterfield. Oxford University Press, New York, http://www.perseus.tufts.edu/hopper/text?doc=Perseus%3Atext%3A1999.01.0126%3Abook%3D1%3Achapter%3D73

- Iversen P. and Jones A., 2019. The Back Plate Inscription and eclipse scheme of the Antikythera Mechanism revisited. *Archive for History of Exact Sciences*, 73, pp. 469–511.

- Jones A., 2017. A Portable Cosmos. Oxford University Press, New York.

- Kircher A., 1646. Ars Magna Lucis et Umbrae in Decem Libros Digesta, Romæ: Sumptibus Hermanni Scheus; Ex typographia Ludouici Grignani. http://lhldigital.lindahall.org/cdm/ref/collection/color/id/23013

- Lazos C., 1994. The Antikythera Computer, Aiolos Publications, Athens.

- Lehoux D.R., 2012. Astronomy, Weather, and Calendars in the Ancient World: Parapegmata and related texts in Classical and Near Eastern Societies. Cambridge University Press, Cambridge.

- Meeus J., 1998. Astronomical Algorithms. 2nd Edition, Willmann-Bell, Virginia.

- Meeus J., 2004. Mathematical Astronomy Morsels III. Willmann-Bell, Virginia.

- Meeus J., Grosjean, C.C., and Vanderleen, W., 1966. Canon of Solar Eclipses. Pergamon Press, Oxford, United Kingdom.

- Neugebauer O., 1975. A History of Ancient Mathematical Astronomy. Springer-Verlag, Berlin; NewYork.

- Nickiforov M.G., 2011. On the discovery of the Saros. Bulgarian Astronomical Journal 16, pp. 72–90.

- von Oppolzer T.R., 1889. Canon der Finsternisse. Wien.

- Panchenko D., 1994. Thales's Prediction of a Solar Eclipse. *Journal for the History of Astronomy*, 25(4), pp. 275–288.

- Pedersen O., 2011. A Survey of the Almagest, Sources and Studies in the History of Mathematics and Physical Sciences. Springer, London; New York; Dordrecht; Heidelberg.

- Price D.S., 1974. Gears from the Greeks: The Antikythera Mechanism, a Calendar Computer from ca. 80 B.C. *Trans. Am. Phil. Soc*. 64(7), pp. 1–70.

- Ptolemy C., 1984. Syntaxis Mathematica. In: Toomer G.J. (ed.). Duckworth Classical, Medieval and Renaissance Editions, London.

- Seiradakis J.H., 2018. The Antikythera Mechanism: Decoding an astonishing 2000 years old astronomical computer, Talk: in CERN, Geneva, (23 March 2018) https://cds.cern.ch/record/2310386?ln=el , on slides 184–237.

- Starry Night software https://starrynight.com/starry-night-8-professional-astronomy-telescope-control-software.html

- Steele J.M., 2000. Eclipse Prediction in Mesopotamia, *Archive for History of Exact Sciences*, 54, pp. 421–54.

- Steele J.M., 2000. A Re-analysis of the Eclipse Observations in Ptolemy's Almagest. *Centaurus*, 42, pp. 89–108.

- Steele J.M., 2015. Eclipses: Calculating and Predicting Eclipses. In: Selin H. (eds), Encyclopaedia of the History of Science, Technology, and Medicine in Non-Western Cultures. Springer, Dordrecht.

- Steele J.M., 2002. A Simple Function for the Length of the Saros in Babylonian Astronomy. In: Steele J.M. and Imhausen A. (eds), Under One Sky: Astronomy and Mathematics in the Ancient Near East. Ugarit-Verlag, Münster, pp. 405–420.

- Stephenson R.F. and Fatoohi L.J., 1997. Thales's Prediction of a Solar Eclipse, *Journal for the History of Astronomy*, 28(4), pp. 279–282.

- The Great American Eclipse, https://www.greatamericaneclipse.com/basics

- Theodosiou S. and Danezis M., 1995. The Calendar Odyssey, in Greek. Diaylos, Athens.

- Vaughan V., 2002. The Origin of the Olympics: Ancient Calendars and the Race Against Time. One Reed Publications, Massachusetts.

- Voulgaris, A.; Vossinakis, A., and Mouratidis, C., 2018a. The New Findings from the Antikythera Mechanism Front Plate Astronomical Dial and its Reconstruction. *Archeomatica International*, Special Issue 3(8), pp. 6–18. https://www.yumpu.com/en/document/view/59846561/archeomatica-international-2017.

- Voulgaris, A.; Mouratidis, C., and Vossinakis, A., 2018b. Conclusions from the Functional Reconstruction of the Antikythera Mechanism. *Journal for the History of Astronomy*, 49(2), pp. 216–238.

- Voulgaris, A.; Vossinakis, A., and Mouratidis C., 2018c. The Dark Shades of the Antikythera Mechanism. *Journal of Radioanalytical and Nuclear Chemistry*, 318, pp. 1881–1891.

- Voulgaris, A.; Mouratidis, C., and Vossinakis A., 2019a. Ancient Machine Tools for the Construction of the Antikythera Mechanism parts. *Digital Applications in Archaeology and Cultural Heritages Journal*, 13, e00092, pp. 1–12.

- Voulgaris, A.; Mouratidis, C., and Vossinakis, A., 2019b. Simulation and Analysis of Natural Seawater Chemical Reactions on the Antikythera Mechanism. *Journal of Coastal Research*, 35(5), pp. 959–972.

- van der Waerden B.L., 1984b. Greek Astronomical Calendars. II. Callipus and his Calendar. *Archive for History of Exact Sciences*, 29, pp. 115–24.

- Williams College Solar Eclipse Expeditions, https://sites.williams.edu/eclipse/2019-chile/

- Wright, M.T., 2005. The Antikythera Mechanism: a New Gearing Scheme. *Bulletin of the Scientific Instrument Society*, 85, pp. 2-7.

- Wright M.T., 2006. The Antikythera Mechanism and the Early History of the Moon-Phase Display, *Antiquarian Horology*, 29(3), pp. 319–329.

- Wright, M.T., 2011. The Antikythera Mechanism: Reconstruction as a medium for research and publication. In: Staubermann, K. (ed.), Reconstructions: Recreating Science and Technology of the Past. Edinburgh, United Kingdom: National Museums Scotland NMS Enterprises Limited, pp. 1–20.

Wright M.T., 2012. The Front Dial of the Antikythera Mechanism, in T. Koetsier and M. Ceccarelli (eds), *Explorations in the History of Machines and Mechanisms* (Dordrecht: Springer), pp. 279–92.